Relativistic Neutron Stars in General Relativity and Fourth Order Gravity.

Nkosinathi Masetlwa

THESIS PRESENTED FOR THE DEGREE OF MASTER OF SCIENCE IN THE DEPARTMENT OF MATHEMATICS AND APPLIED MATHEMATICS AT THE UNIVERSITY OF CAPE TOWN.
DECEMBER 2020.

Supervisor:
Dr. Bishop Mongwane
Department of Mathematics and Applied Mathematics, University of Cape Town

Co-Supervisors:
Dr. Kurt van der Heyden
Department of Astronomy, University of Cape Town
& South African Astronomical Observatory & National Research Foundation

and Prof. Amanda Weltman
Department of Mathematics and Applied Mathematics, University of Cape Town

Abstract

This thesis investigates numerical instabilities arising from stiffness in the models of non-rotating, spherically symmetric single neutron star systems. The work deals with two distinct problems, each of which involves a stiff system of differential equations. In each case, we deal with stiffness by employing an IMEX Runge-Kutta scheme as opposed to the more computationally intensive fully implicit schemes or other adaptive Runge Kutta methods that may be impractical for partial differential equations. The first problem is focused on the mass-radius relation of a neutron star under a quadratic $f(R) = R + \alpha R^2$ theory for various realistic equations of state. This results in a coupled system of ODEs with stiff source terms which we discretize using an IMEX scheme. The observed maximum masses for different values of α, were consistent with the current neutron star maximum mass limit for some equations of state in both GR and beyond. In the second problem, we compute the frequencies of radial oscillations of neutron stars in the context of general relativity. This is achieved by linearly perturbing the ADM equations coupled to a matter source term. We discretize the resulting coupled system of PDEs with a third order WENO scheme in space and an IMEX scheme in time. We obtained 18 frequencies from the Fast Fourier Transform (FFT) of the evolved perturbation equations, which were consistent with the frequencies of the neutron star's Sturm-Liouville problem. The efficiency of the IMEX scheme as compared to other methods such as fully implicit schemes or adaptive methods makes it ideal for implementation in fully 3D numerical relativity codes for modified gravity.

Contents

Chapter 1

Introduction

There has been vast development in the field of astronomy and astrophysics in the past century ever since the theory of a static universe was disproved. These results include the Supernovae type Ia data [1, 2], Large scale structure surveys [3], and the cosmic microwave background data [4] that verified an accelerating universe dominated by dark matter and dark energy. These surveys presented data that verified cosmological models with an expanding universe described in them. Specifically, the ΛCMD model which comes with the additional mystery of dark energy and dark matter. Intensive research has ever since been focused into investigating the nature of the 74.2% of dark energy that is responsible for the cosmic expansion and the 21.4% of dark matter in the universe. To this point, the list of the candidates *e.g* [5, 6], behind dark matter is still being tested and they currently account for the smallest masses $10^{-22}\ eV$ to the largest masses $10^{72}\ eV$ speculated in the universe.

The nature of dark energy on the other hand has led to research that aims to understand the pull behind the acceleration of the universe, which in the simplest general relativity model is attributed to the cosmological constant. When we view the universe from quantum field theory, we get a beautiful picture that explains particle interactions and the forces that binds them. In quantum gravity, the cosmological constant's equivalence is associated with the lowest energy state of a vacuum system and the theory estimates the energy to be in $\sim 10^2$ orders of magnitude. Quantum field theory estimates the value of the cosmological constant to be higher than speculated in general relativity. Hence, the long standing Einstein's theory of general relativity evidently has more limitations in addition to its lack of accountability for the early inflation. This is one of the obstacles that stand in the way of having a unified theory of everything.

This point is bittersweet to researchers. As the present tools become less adequate, the search for better tools gets intensive. This is seen with the influx of alternate theories to general relativity, that aim to explain the cosmic acceleration observed. These theories include scalar-field theories such as Quintessense, introducing an additional potential to the Einstein's equations; brane-world theories where gravity is governed by super-massive gravitons; and Fourth order gravity theories where gravity is modified by means of introducing a nonlinear Ricci scalar function $f(R)$ to Einstein's Lagrangian. There is an ocean of these theories and they all present some contending points along with their shortcomings of course. These theories need to recover general relativity when tested in the solar system and laboratory tests for them to be validated, see [7, 8] - and references therein - for a broader review of these alternative theories.

Fourth order gravity theories were first introduced as a geometrical interpretation of gravity, that was supposed to be an alternate to the Einstein's theory by Weyl [9]. Although it was refuted by Einstein at the time, it later garnered attention due to its inclusion of higher-order curvature invariants with respect to the Ricci scalar in the Einstein-Hilbert action. The fourth order gravity terms seemed to solve the early universe singularity problem and inflationary epoch, which made them more desirable by researchers. Since then, there has been an incredible amount of activity in researching these models, hence there currently exists more higher order gravity theories *e.g* [10]. Some of these models have failed the necessary viability conditions, but there are few models that are consistent with current cosmological constraints and solar system dynamics. The two widely used models within the $f(R)$ class of theories are, the Hu-Sawicki model [12] which introduces broken power laws with respect to the Ricci scalar, and the Starobinsky model [122] which introduces quadratic Ricci scalar terms.

Testing these modified gravity theories in the solar system only provides the model with constraints in the weak-field regime. However, the most complex and equally pertinent part is the strong field regime. Black holes and neutron stars are some of the best laboratory tests for strong field limits, due to their extreme gravitational nature. Hence, testing modified gravity theories in these limits, remains the best option to constrain and possibly rule out some of the viable models.

The drawback with testing modified gravity theories under neutron stars is that, there is no universal equation of state (EoS) accurately describing the internal matter. During the past decades there has been a vast number of EoS being proposed and still counting - see [13] for a list - some of which produce results consistent with current observations. Constraining these EoS, requires some observational data from neutron stars. Fortunately, we now live in an epoch where neutron star's gravitational waves are not only theorized but measured [14–16]. This follows from one of the most celebrated events taking place at the Advanced LIGO and Virgo institutes, where the first gravitational wave signal GW170817, from the inspiral and merger of a binary neutron-star system [130] was detected. The more recent gravitational wave detection GW190814 by the same institutions, occurred in 2019 where a black hole was observed to merge with a compact object [17]. The detection GW170817 shed some light on neutron stars, where the upper bound of their maximum mass was refined to $2.3M_{\odot}$ [18, 131]. Although the second compact object was unidentified in the GW190814 detection, its observed mass is around $2.6M_{\odot}$. If it was a black hole then it must be a very small one, and if it was a neutron star, it sets a new maximum mass limit. These gravitational wave detections have helped constrain the already existing modified gravity theories [19–21], and they help in constructing new theories [22]. Further simulating the strong field regime requires efficient and accurate relativistic codes. Nonlinear relativistic codes have had difficulties when extended to multi-dimensions, ultra-relativistic regimes, or handling evolution discontinuities. Nevertheless, advancements in supercomputer technology is making it possible to probe these fields with higher order relativistic codes [23–25].

Problem Identification

Stiffness is a barrier to stable numerical evolutions of modified gravity theories. For example, in $f(R)$ gravity, the ADM equations for the scalar field contain terms that are proportional to $1/f''$. This poses a problem for the $f(R)$ theories that are closer to GR as they satisfy

$f'' \to 0$. Leading to instabilities in the spacetime evolution of these theories. These are often treated by using adaptive step-size Runge-Kutta methods, which are efficient and accurate for ODEs. However, these are not practical for large scale numerical simulations, especially those involving spatial derivatives in 3D. This behavior can be studied by understanding the model problem

$$\partial_t u = \boldsymbol{Q}(u) + \frac{1}{\tau}\boldsymbol{R}(u). \tag{1.1}$$

which we discuss in Chapter 5. In this thesis, we focus on the following two problems that contain stiff terms similar to the scalar field equations in $f(R)$:

- The first part arises in the TOV equations of $f(R)$ gravity. Non-rotating static spherically symmetric neutron stars have been studied in the context of $f(R)$ gravity in [125–127]. Our approach in this thesis differs from those in the literature in that we do not use adaptive Runge-Kutta methods. We instead employ an IMEX scheme to handle the stiffness. This is detailed in Chapter 5.

- The second problem focuses on radial oscillations of relativistic stars. Radial oscillations of relativistic stars have been studied widely over the years [146, 152, 153]. Our approach in this thesis differs from existing approaches in that *i*) We solve a coupled system of PDEs instead of the usual Sturm-Liouville form and *ii*) We use a third order WENO shock capturing scheme coupled to the IMEX scheme as opposed to the Lax-Wendroff scheme (used in [148]) and McCormac scheme (used in [149]). This is detailed in Chapter 6.

This thesis is organized as follows: In chapter 2, we briefly introduce the Einstein field equations. Further, we review the metric $f(R)$ gravity and its equivalence with a scalar-field theory. In chapter 3, we recast the evolution equations of the neutron star in a $3+1$ formalism. Additionally, we extend the equations to the BSSN formalism and discuss the gauge conditions that simplify the equations. We also discuss the evolution of the neutron star's matter. In chapter 4, we present the numerical methods that are relevant to the work in this thesis. We present both low order and higher order methods, and discuss some of their efficiency and stability. In chapter 5 we focus on neutron stars in the $R - squared$ gravity. We evolve the modified TOV equations under 7 different equations of state. We further provide the $\mathcal{M} - \mathcal{R}$ relations for each EoS, then discuss their gravitational mass and maximum mass for different values of α. In chapter 6 we focus on the radial oscillations of a neutron star in general relativity with a polytropic equation of state. We perturb the ADM equations and evolve the resulting linearized field equations. Additionally, we solve the Sturm-Liouville problem which gives eigenfrequencies to verify against.

Notations and Conventions

- We used the signature $(-,+,+,+)$ for the metric.
- We assume geometrized units such that G=c=1.
- Primes are used to show derivatives with respect to the radial coordinate r *e.g* g' with the exception of f′, f′′ and f′′′, which denote derivatives with of the function f(R) with respect to the Ricci scalar.

Chapter 2

Preliminaries

2.1 Einstein's Field Equations

The theory of general relativity explains gravitational interactions in the universe, although with some limitations. In the following, we give a brief overview of some of the relevant concepts of general relativity employed in this thesis. A more in-depth treatment of these topics can be found in e.g. [28, 30]. It states that the spacetime has a 4-d metric denoted by g_{ab}, which determines the invariant interval distance ds^2 between two 4-dimensional events on the spacetime. This line element is given by

$$ds^2 = g_{ab}dx^a dx^b. \tag{2.1}$$

In this spacetime we can measure how a tensor A^b_a changes when you parallel transport it throughout the spacetime i.e *keep it constant while transporting it along some path*. This change is measured using the covariant derivative which is

$$\nabla_c A^b_a = \partial_c A^b_a + \Gamma^b_{dc} A^d_a - \Gamma^d_{ac} A^b_d, \tag{2.2}$$

where Γ^a_{bc} are the Christoffel symbols that are associated with the metric g_{ab} and they determine the change in the basis vectors and their co-vectors of the coordinate basis with respect to parallel transport, and these functions are given by the equations

$$\Gamma^a_{bc} = \frac{1}{2} g^{ad}(\partial_b g_{dc} + \partial_c g_{bd} - \partial_d g_{bc}), \tag{2.3}$$

where g^{ab} is the inverse of the metric such that

$$g_{ab}g^{ab} = \delta^b_a. \tag{2.4}$$

All this ground work is valid in both curved and flat spaces, as the metric g_{ab} in flat spaces becomes the Minkowski metric

$$\eta_{ab} = diag(-1, 1, 1, 1). \tag{2.5}$$

Now when we extend our theory into curved space, one of the key variables that explains curvature in the gravitational field is the Riemann curvature tensor R^a_{bcd} which is given by

$$R^a_{bcd} = \partial_c \Gamma^a_{bd} - \partial_d \Gamma^a_{bc} + \Gamma^a_{ec}\Gamma^e_{bd} - \Gamma^a_{ed}\Gamma^e_{bc}, \tag{2.6}$$

which vanishes in flat space *i.e* $g_{ab} = \eta_{ab}$. One of the properties of the Riemann tensor is the sum of cyclic permutations of its lowered version's first three indices in that

$$\nabla_a R_{bcde} + \nabla_b R_{cade} + \nabla_c R_{abde} = 0, \tag{2.7}$$

and due to the anti-symmetry of the Riemann in its first two indices i.e $R_{bcde} = -R_{cbde}$, we have the Bianchi identity

$$\nabla_{[a} R_{bc]de} = 0. \tag{2.8}$$

When we contract the Riemann tensor along the upper indice and one of the lower indices we get a symmetric rank-2 tensor called the Ricci tensor

$$R_{ab} = R^c_{abc}. \tag{2.9}$$

The trace of the Ricci tensor is so special due to its symmetries that it is called the Ricci scalar

$$R = R^a_a, \tag{2.10}$$

which is also sometimes referred to as the curvature scalar.

Let us consider the Bianchi identity contracted twice with the inverse of our metric as

$$g^{ec} g^{ad} (\nabla_a R_{bcde} + \nabla_b R_{cade} + \nabla_c R_{abde}) = 0, \tag{2.11}$$

which after contracting along $a = e$ we get

$$\nabla^a (2R_{ba} - g_{ab} R) = 0, \tag{2.12}$$

the expression inside the parentheses is called the Einstein tensor which its symmetry is inherited from that of the Ricci tensor. Which is clearly defined as

$$G_{ab} = R_{ab} - \frac{1}{2} R g_{ab}. \tag{2.13}$$

The Einstein tensor G_{ab} is related to the Energy momentum tensor T_{ab} via

$$G_{ab} = \kappa T_{ab}. \tag{2.14}$$

In the weak-field limit the Einstein's equations are required to reduce to the Poisson equation, which fixes κ to be 8π in Geometrized units (G=c=1). The conservation equations take the form

$$\nabla^a T_{ab} = 0. \tag{2.15}$$

For a perfect-fluid the energy-momentum tensor is defined as

$$T_{ab} = (\rho + p) U_a U_b + p g_{ab}, \tag{2.16}$$

where ρ is the matter energy density, p is the momentum density in the frame, and the four-velocities U_a are timelike vectors. Through the comparison of the components we obtain the Einstein Field equations

$$R_{ab} - \frac{1}{2} R g_{ab} = 8\pi T_{ab}. \tag{2.17}$$

2.2 Metric f(R) gravity

There is another way of deriving the field equations (2.17), where they interpreted as equations of motion from a Lagrangian density in the gravitational field. This method was first studied in depth in [33]. The Lagrangian density for General Relativity can be written as a function of the Ricci scalar such that

$$f(R) = R. \tag{2.18}$$

We can obtain the Einstein-Hilbert action $\mathcal{S}$ for the gravitational field, from the spacetime metric $\mathcal{S}$ denoted by

$$\mathcal{S} = \frac{1}{16\pi}\int d^4x[f(R)\sqrt{-det(g_{ab})}] + \mathcal{S}_{matter}(g_{ab}, \Phi), \tag{2.19}$$

in natural units and where $\mathcal{S}_{matter}$ is the action for ordinary matter fields. We vary the action with respect to the inverse spacetime metric g^{ab}, which leads to the general field equations

$$f'(R)R_{ab} - \frac{1}{2}f(R)g_{ab} - [\nabla_a\nabla_b - g_{ab}\Box]f'(R) = 16\pi T_{ab}, \tag{2.20}$$

where the prime denoted the derivative of the Lagrangian density with respect to the Ricci scalar i.e df/dR and the d'Alembertian is the usual $\Box = \nabla_a\nabla^a$. it is obvious that for the case $f(R) = R$, these equations reduce to the Einstein field equations (2.17) (with $\Lambda \approx 0$). To complete these equations the energy-momentum tensor takes the form

$$T_{ab} = \frac{-2}{\sqrt{-g}}\frac{\delta\mathcal{S}_{matter}}{\delta g^{ab}}. \tag{2.21}$$

Furthermore, in $f(R)$ gravity this energy-momentum tensor still obeys the vanishing covariance divergence $\nabla_a T^{ab} = 0$, as shown in [34].

Contracting the general field equations (2.20) with the inverse metric g^{ab}, we find a more general relation between the Ricci scalar R and the trace of the energy-momentum tensor $T = g^{ab}T_{ab}$ where

$$f'R - 2f(R) + 3\Box f'(R) = 8\pi T, \tag{2.22}$$

where in the $f(R) = R$ case a vanishing Ricci scalar ($R = 0$) implied a vanishing energy-momentum trace ($T = 0$), which is not the case in this modified theory of gravity.

2.2.1 Equivalence with Brans-Dicke Gravity

The Brans-Dicke (BD) theories of gravity [35] are one of the extensions of Einstein's general relativity, they a form of scalar-tensor theories. The metric $f(R)$ gravity theories have been proven to be a special case equivalence of the Brans-Dicke theories [36–39] with the Brans-Dicke parameter $\omega_{BD} = 0$. This can be seen from the action (2.19) for metric $f(R)$ gravity by introducing a new field χ and rewrite the dynamically equivalent action in the form

$$\mathcal{S} = \frac{1}{16\pi}\int d^4x[f(\chi)\sqrt{-det(g_{ab})} - f'(\chi)(R-\chi)] + \mathcal{S}_{matter}(g_{ab}, \Phi). \tag{2.23}$$

We obtain the dynamic equations by varying the action (2.23) with respect to the field χ, which leads to the equation

$$f''(\chi)(R-\chi) = 0. \tag{2.24}$$

Therefore, the two theories are equivalent *i.e* $R = \chi$, if $f''(\chi) \neq 0$, which reduces (2.23) to the metric $f(R)$ gravity's action. Suppose we define an auxiliary field

$$\phi = f'(\chi), \tag{2.25}$$

and then we introduce a potential function

$$V(\phi) = \chi(\phi)\phi - f(\chi(\phi)). \tag{2.26}$$

The action can then be rewritten in the form

$$\mathcal{S} = \frac{1}{16\pi}\int d^4x\sqrt{-det(g_{ab})}[\phi R - V(\phi)] + \mathcal{S}_{matter}(g_{ab}, \Phi), \tag{2.27}$$

which is an action associated with a non-dynamic field ϕ in a Jordan frame representation, within the context of a Brans-Dicke theory [36].

Chapter 3

The 3+1 Formalism

3.1 The 3+1 Decomposition

We have an interest in numerically solving the Einstein field equations (2.17) to model spacetime dynamics under configurations of interest. In the previous chapter we showed an analytical way to reduce the covariant field equations into coupled ordinary differential equations that can be solved numerically to recover the metric of a TOV neutron star (5.1). In this chapter we will look at other formulations that allow us to solve them in 3-dimensions and evolved them through time to create our spacetime. To do this we will need to have initial data and some boundary conditions of the spacetime, and use the evolution equations of the variables of the field equations to look into the future/past of the system. Currently we have to solve ten coupled non-linear partial differential equations, and space and time are handled similarly as coordinates when we have the field equations in this covariant form. Solving that kind of a system numerically is computational expensive but it would be better to have the problem rewritten as a Cauchy problem, one formulation based on splitting the spacetime into a $\{3+1\}$-dimensional universe, introduced by York in [41] does help us achieve this. We want to express the system as a reduced boundary value problem by slicing the spacetime into hypersurfaces distinguished by Σ_t where t is constant throughout the hypersurface, this formulation is called the ADM-formulation named introduced by Arnowitt, Deser, and Misner in [42].

The ADM formulation has been the standard in solving the field equations. Its general idea is that we split the field equations into spatial and temporal equations. We achieve this by describing our spacetime with metric g_{ab} as a 1-dimensional foliation of the 3-dimensional hypersurfaces Σ_t, such that the next hypersurface is denoted by Σ_{t+dt}. We make the assumption that all the points on these hypersufaces are related to each other spatially only, and that makes them Cauchy surfaces [43]. We consider two neighboring hypersurfaces Σ_t and Σ_{t+dt} as shown in figure (3.1), on these hypersurfaces let us consider two observers situated at $x^i(t)$ on Σ_t, such that for these observers on Σ_{t+dt} we would like to know:

- The proper distance dl^2 between them, which can be defined with the $3-d$ metric on the sheet denoted by λ_{ij}, such that

$$dl^2 = \gamma_{ij} dx^i dx^j \qquad i,j = 1,2,3$$

.

- If we suppose that one of the observers moves in a normal direction to the hypersurfaces $i.e$ an Eulerian observer, the proper time $d\tau$ for this observer will be defined by the lapse function α such that

$$d\tau = \alpha(t, x^i)dt$$

.

- For our non-Eulerian observer, their position on Σ_{t+dt} can be denoted by $x^i(t+dt)$ which can be obtained from the relative velocity of the Eulerian observer β^i as

$$x^i(t + dt) = x^i(t) + \beta^i dt$$

.

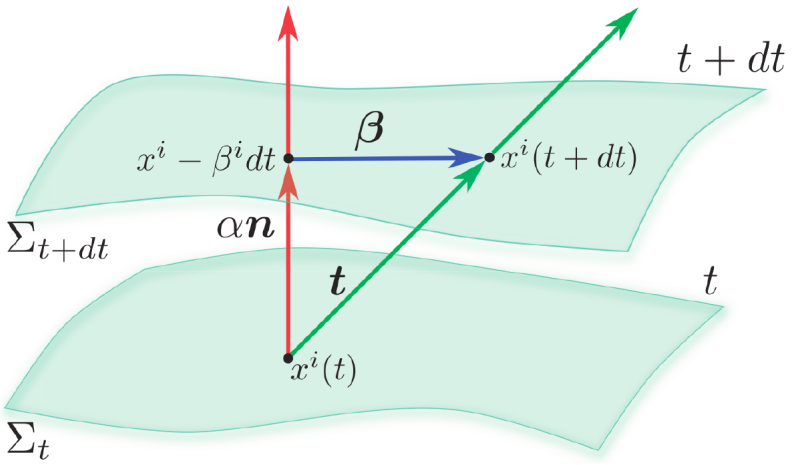

Figure 3.1: The $3 + 1$-spacetime foliation and the relation between the hypersurfaces Σ_t and Σ_{t+dt} [44].

Now if we take a Lie derivative of any tensor along the vector **t**, we recover the "rate of change of the tensor" from Σ_t to Σ_{t+dt} [45], and we can define the "time vector" which is tangent to the world line of our non-Eulerian observer by the unit vector

$$t^a = \alpha n^a + \beta^a, \tag{3.1}$$

where $a = 0, 1, 2, 3$. This vector has the property of duality $t^a \nabla_a t = 1$, shows us the change of t along t^a a constant value everywhere on the hypersurface Σ_t.The vector n^a is a $4 - d$ vector perpendicular to the hypersurfaces which we refer to as the normal vector and it is denoted by [46]

$$n^a = \left(\frac{1}{\alpha}, -\frac{\beta^i}{\alpha}\right), \tag{3.2}$$

and its one-form is

$$n_a = (-\alpha, 0^i). \tag{3.3}$$

Our observers could have numerous world lines between the hypersurfaces, and it shows that they are determined by the relative velocity - which is referred to as the shift vector - β^i and the lapse function α. These are our gauge functions which we can set conditions for to describe

the foliation of our spacetime. From the equation (3.2) we can obtain the acceleration of our Eulerian observer as

$$n^a \nabla_a n_i = \partial_i ln\alpha, \tag{3.4}$$

but a certain property of the normal vector is

$$n^b n^a \nabla_a n_b = 0,$$

hence

$$n^b \partial_i ln\alpha = 0, \tag{3.5}$$

would mean that for $\alpha = constant$, the Eulerian observer is free falling through their normal world line.

The spatial variables' contravariant components can be found by lowering or raising their indices with the spatial metric γ_{ij} and its inverse γ^{ij}, then we have $\beta_i = \gamma_{ij}\beta^j$. In our coordinate system the time vector is unit timelike vector $i.e$ $\mathbf{t} = \partial_t$ and we can obtain the 4-metric components in this system, knowing that the spatial components are just equal to the metric of the hypersurfaces, that is

$$g_{ij} = \partial_i \cdot \partial_j, \tag{3.6}$$
$$g_{ij} = \gamma_{ij}. \tag{3.7}$$

The temporal component of the metric is

$$g_{tt} = \partial_t \cdot \partial_t \tag{3.8}$$
$$= (\alpha n^a + \beta^a) \cdot (\alpha n^a + \beta^a), \tag{3.9}$$

where we used the equation (3.1) and also recalling that the shift vector is purely spatial, this gives us

$$g_{tt} = -\alpha^2 + \beta^i \cdot \beta_i. \tag{3.10}$$

Then now the last remaining terms of the 4-metric

$$g_{ti} = \partial_t \cdot \partial_i, \tag{3.11}$$

which one can show that it is simply

$$g_{ti} = \beta_i. \tag{3.12}$$

We have now presented the decomposed version of our differential line element for the spacetime using all the aforementioned variables as

$$ds^2 = (\beta^i \beta_i - \alpha^2)dt^2 + 2\beta_i dt dx^i + \gamma_{ij} dx^i dx^j. \tag{3.13}$$

We can write our 4-metric more explicitly as

$$g_{ab} = \begin{pmatrix} \beta^i \beta_i - \alpha^2 & \beta_i \\ \beta_j & \gamma_{ij} \end{pmatrix}, \tag{3.14}$$

and its inverse

$$g^{ab} = \begin{pmatrix} -1/\alpha^2 & \beta_i/\alpha^2 \\ \beta_j/\alpha^2 & \gamma^{ij} - \beta^i \beta^j/\alpha^2 \end{pmatrix}. \tag{3.15}$$

The foliation of the spacetime induces the $3-d$ metric γ_{ij} on the hypersurfaces, which is defined

$$\gamma_{ab} = g_{ab} + n_a n_b, \tag{3.16}$$

and its inverse can be found by contracting through both its indices using the inverse of the 4-metric such that

$$\gamma^{cd} = g^{ac} g^{bd} \gamma_{ab}, \tag{3.17}$$
$$\gamma^{cd} = g^{cd} + n^c n^d. \tag{3.18}$$

One thing that is obvious but worth noting is that the spatial metric will have its projection along the normal vanish, that is

$$\gamma_{ab} n^a = 0. \tag{3.19}$$

Lastly, something to mention about this variable is that its determinant is related to the 4-metric's determinant through the lapse function as

$$\sqrt{-det(g_{ab})} = \alpha \sqrt{det(\gamma_{ij})}, \tag{3.20}$$

which tells us more about the physical volume per coordinate volume.

3.2 Extrinsic Curvature

We now know more about the metric of our hypersurfaces, one other question we could ask is regarding the change of the normal vector when parallel transported around the hypersurface Σ_t knowing that we are not assuming flat 3-d spacetime on the sheets. To learn more about this change, we would have to look at the spatial projections of this change in the normal on the hypersurface, that is the term

$$\gamma^a_e \gamma^b_d \nabla_a n_b. \tag{3.21}$$

Here we project with the rank-$\binom{1}{1}$ spatial metric since it projects everything along the normal onto the hypersurfaces defined by raising the spatial metric's index by the 4-metric and more explicitly as $\gamma^a_b = \delta^a_b + n^a n_b$.

This term (3.21) generally tells about the curvature of the hypersurfaces due to living in the 4-d spacetime with metric g_{ab}, throughout t. Let us split the term into its symmetric and anti-symmetric parts as

$$\phi_{ab} = \gamma^a_e \gamma^b_d \nabla_{(a} n_{b)}, \tag{3.22}$$
$$\tau_{ab} = \gamma^a_e \gamma^b_d \nabla_{[a} n_{b]}, \tag{3.23}$$

respectively. The negative of the symmetric term is called the extrinsic curvature of the hypersurface, which is denoted by

$$K_{ab} =: -\gamma^a_e \gamma^b_d \nabla_{(a} n_{b)}, \tag{3.24}$$

which is a purely spatial that is any projection of it along the normal vanishes $i.e\ n^a K_{ab} = n^b K_{ab} = 0$ and it is also a symmetric tensor $i.e K_{ab} = K_{ba}$.

If we consider the difference between the changes of the spatial metric γ_{ab} along the normal, which tells us also about the way the hypersurfaces are immersed in the 4-d spacetime. This is

the Lie derivative of the spatial metric and as it should come to no surprise from the definition that we find the relation between it and the extrinsic curvature

$$K_{ab} = -\frac{1}{2}\mathcal{L}_{\mathbf{n}}\gamma_{ab}. \tag{3.25}$$

We realise from here that we can actually define the extrinsic curvature as the "velocity" of the spatial metric as measured by our Eulerian observer. More interestingly enough is that one can measure the volume of the hypersurface Σ_t from the trace of the extrinsic curvature

$$K = \gamma^{ab}K_{ab}, \tag{3.26}$$
$$K = -\mathcal{L}_{\mathbf{n}}\gamma^{1/2}, \tag{3.27}$$

which we refer to as the mean curvature. Therefore the volume of Σ_t is given by

$$V_t = \sqrt{\gamma}d^3x, \tag{3.28}$$

and from this we note that the extrinsic curvature measures the fractional change in the proper 3-volume along the normal.

The Lie derivative of an arbitrary tensor A^a_b along a vector X^c can be written explicitly as

$$\mathcal{L}_X A^a_b = X^c\nabla_c A^a_b - T^c_b\nabla_c X^a + A^a_b\nabla_b X^c. \tag{3.29}$$

Where in a flat spacetime the covariant derivatives reduces to partial derivatives as the symmetric connections vanishes, rendering

$$\mathcal{L}_i = \partial_i, \tag{3.30}$$
$$\mathcal{L}_t = \partial_t, \tag{3.31}$$

in these coordinates. Suppose we consider a scalar function f that is defined on the hypersurface Σ_t, then with this newly defined arbitrary function we have

$$\mathcal{L}_{\mathbf{n}}\gamma_{ab} = \frac{1}{f}\mathcal{L}_{f\mathbf{n}}\gamma_{ab}. \tag{3.32}$$

To make use of this property, let us suppose our scalar function here is the lapse function α then we will have

$$\mathcal{L}_{\mathbf{n}}\gamma_{ab} = -\frac{1}{2\alpha}\mathcal{L}_{\alpha\mathbf{n}}\gamma_{ab} \tag{3.33}$$
$$= -\frac{1}{2\alpha}\Big(\mathcal{L}_{\mathbf{t}} - \mathcal{L}_{\boldsymbol{\beta}}\Big)\gamma_{ab}, \tag{3.34}$$

where we used the equation (3.1) to decompose our lapse function. Now meaning that when we return to our adapted coordinates in the hypersurface, the above equation reduces to

$$\partial_t\gamma_{ij} - \mathcal{L}_{\boldsymbol{\beta}}\gamma_{ij} = -2\alpha K_{ij}, \tag{3.35}$$

which gives us an evolution equation for the spatial metric of the hypersurfaces. Defining a three dimensional projection of the four dimensional covariant derivative onto the hypersurface as $D_a =: \gamma^b_a\nabla_b$ allows us to rewrite the evolution equation as

$$\partial_t\gamma_{ij} = -\alpha K_{ij} + D_i\beta_j + D_j\beta_i, \tag{3.36}$$

which only depends on the extrinsic curvature and the normal vector in the hypersurface.

3.3 Constraint Equations

At this point we realise that our spacetime foliation is determined by the pair of tensors (γ_{ij}, K_{ij}). Before we can extend this formalism into the Einstein field equations, the spatial metric and the extrinsic curvature need to satisfy certain constraint equations which is our intention in this section. First let us look at a couple of projections of the 4-d Riemann tensor ${}^{(4)}R_{abcd}$ in our spacetime onto the hypersurface Σ_t,

$$\gamma_d^s\gamma_a^p\gamma_b^q\gamma_c^{r\,(4)}R_{srqp} = {}^{(3)}R_{abcd} + K_{ac}K_{bd} - K_{ad}K_{cb}, \tag{3.37}$$

this is called the *Gauss-Codazzi equations*. Suppose now we contract one index of the 4-d Riemann tensor along the normal vector of the hypersurface, that is projecting towards the "positive" time direction we obtain

$$\gamma_a^p\gamma_b^q\gamma_c^r n^{s\,(4)}R_{srqp} = D_bK_{ac} - D_aK_{bc}. \tag{3.38}$$

The spatial derivative of the extrinsic curvature in this direction is defined as

$$D_aK_{bc} = \gamma_a^p\gamma_b^q\gamma_c^r\nabla_pK_{qr}, \tag{3.39}$$

and the equations (3.38) are called the *Codazzi-Mainardi*. Lastly we take it further and project two indices of the 4-d Riemann tensor onto the normal direction, this after some manipulation gives us

$$\mathcal{L}_{\mathbf{n}}K_{ab} = n^dn^c\gamma_a^q\gamma_b^{r\,(4)}R_{drcq} - \frac{1}{\alpha}D_aD_b\alpha - K_b^cK_{ac}, \tag{3.40}$$

which is basically the evolution equation of the extrinsic curvature along the normal direction and these are called the *Ricci's equations*.

These equations will help us into writing the Einstein equation into the $3+1$ form, looking at the *Gauss-Codazzi* equations (3.37) and contracting twice gives us

$$\gamma^{sq}\gamma^{pr\,(4)}R_{sqpr} = R - K^{cd}K_{cd} + K^2, \tag{3.41}$$

and using the relation $\gamma_b^a = g_b^a + n^an_b$ this equation reduces to

$${}^{(4)}R + 2n^pn^{r\,(4)}R_{pr} = R - K^{cd}K_{cd} + K^2. \tag{3.42}$$

On the other hand contracting the Einstein's equations (2.13) twice along the normal direction gives us

$$2n^pn^rG_{pr} = 2n^pn^{r\,(4)}R_{pr} + {}^{(4)}R, \tag{3.43}$$

now our normal observer will be measuring the energy density as

$$\rho = n^an^bT_{ab}. \tag{3.44}$$

Then substituting in our Einstein's tensor and using the contracted *Gauss-Codazzi* equation we obtain

$$R - K^{cd}K_{cd} + K^2 = 16\pi n^an^bT_{ab}, \tag{3.45}$$

this is a constraint that must be satisfied by the extrinsic curvature, it is referred to as the *Hamiltonian* constraint.

For the next constraint, let us consider contracting the *Codazzi-Mainardi* equations (3.38) over one index to obtain

$$D_b K_a^b - D_a K = -\gamma_a^p n^{s(4)} R_{ps}, \tag{3.46}$$

where K is the trace of the extrinsic curvature *i.e the mean curvature*. Once again contracting the Einstein's equations gives us

$$\gamma_a^p n^s G_{ps} = \gamma_a^p n^{s(4)} R_{ps}. \tag{3.47}$$

Suppose we define the momentum density measured by our Eulerian observer as

$$S_a = -\gamma_a^b n^c T_{bc}, \tag{3.48}$$

combining the contracted *Codazzi-Mainardi* equations and the momentum density gives the *Momentum* constraint of our system

$$D_b K_a^b - D_a K = 8\pi S_a. \tag{3.49}$$

In our adapted coordinate system the momentum and Hamiltonian constraints we have derived become

$$\begin{aligned} D_j(K_i^j - K) &= 8\pi S_i, & (3.50)\\ R - K^{ij}K_{ij} + K^2 &= 16\pi\rho. & (3.51) \end{aligned}$$

3.4 Evolution Equations

We need to know how the extrinsic curvature and the spatial metric change as we move from one hypersurface to another in their normal direction $i.e$ their time evolution. We see that we already have the extrinsic curvature defined as the Lie derivative of the spatial metric along the normal direction, in equation (3.25) and also we have the Lie derivative of the extrinsic curvature along the normal direction defined in *Ricci's* equation (3.40). Now we like to use these equations to obtain the evolutions in the t^a direction which is our time vector. Let us consider the Lie derivative of the extrinsic curvature along the time vector

$$\begin{aligned} \mathcal{L}_{\boldsymbol{t}} K_{ab} &= \mathcal{L}_{\alpha n+\beta} K_{ab}, & (3.52)\\ &= \alpha \mathcal{L}_n K_{ab} + \mathcal{L}_\beta K_{ab}, & (3.53) \end{aligned}$$

where we used the linear dependence properties of the Lie derivative on the equation of the vector t^a on (3.1). We notice that the first term of the Lie derivative above is a product of the lapse function and the *Ricci's* equation. Now let us consider the first term of the *Ricci's* equation and use the spatial metric's definition (3.16) such that

$$\begin{aligned} n^a n^b \gamma_a^q \gamma_b^{r(4)} R_{dcqr} &= (\gamma^{dc} - g^{dc})\gamma_a^q \gamma_b^{r(4)} R_{dcqr}, & (3.54)\\ &= \gamma^{dc}\gamma_a^q \gamma_b^{r(4)} R_{dcqr} - \gamma_a^q \gamma_b^{r(4)} R_{qr}^{dc}. & (3.55) \end{aligned}$$

If we contract the *Gauss'* equation (3.37) we obtain

$$R_{bd} = \gamma^{pr}\gamma_d^s \gamma_b^{q(4)} R_{dcqr} - K K_{bd} + K_d^c K_{cb}, \tag{3.56}$$

and the Einstein's equations define the 4-d Ricci tensor as

$$^{(4)}R_{ps} = 8\pi T_{ps} + \frac{1}{2}{}^{(4)}Rg_{ps}. \tag{3.57}$$

Substituting the above definition of the 4-d Ricci tensor in equation (3.54) give us

$$n^a n^b \gamma_a^q \gamma_b^r {}^{(4)}R_{dcqr} = R_{ab} - K_a^c K_{cb} + KK_{ab} - 8\pi\gamma_a^q\gamma_b^r(T_{qr} - \frac{1}{2}g_{qr}T). \tag{3.58}$$

Let us define the spatial tress tensor measured by our Eulerian observer as

$$S_{ab} = \gamma_a^c \gamma_b^d T_{cd}, \tag{3.59}$$

and then now looking at the last product term in (3.58), we see that we have $T = T_{ab}g^{ab}$, which we can rewrite as

$$\gamma_a^q\gamma_b^r g_{qr} g^{ef} T_{ef} = \gamma_{ab}(\gamma^{ef} - n^e n^f)T_{ef}. \tag{3.60}$$

Rewriting the projected term in terms of the spatial stress tensor we get

$$\gamma_a^q\gamma_b^r g_{qr} g^{ef} T_{ef} = \gamma_{ab}(S - \rho), \tag{3.61}$$

where $S = g_b^a S_{ab} = S_a^a$ and $\rho = n^a n^b T_{ab}$. Now we substitute the above expressions in ***Ricci's*** equation in (3.52) to obtain

$$\begin{aligned} \mathcal{L}_{\boldsymbol{t}} K_{ab} &= -D_a D_b \alpha + \alpha(R_{ab} - 2K_{ac}K_c^a + KK_{ab}) && (3.62)\\ &- 8\pi\alpha(S_{ab} - \frac{1}{2}\gamma_{ab}(S-\rho)) + \mathcal{L}_{\boldsymbol{\beta}} K_{ab}, && (3.63) \end{aligned}$$

these are the evolution equations of the extrinsic curvature. The evolution equations of the spatial metric can be derived by considering its Lie derivative along the time vector

$$\mathcal{L}_n \gamma_{ab} = \alpha \mathcal{L}_n \gamma_{ab} + \mathcal{L}_\beta \gamma_{ab}. \tag{3.64}$$

Recalling that from equation (3.25) hence this can be considered as a Lie derivative along the temporal direction such that

$$\mathcal{L}_t \gamma_{ab} = -2\alpha K_{ab} + \mathcal{L}_\beta \gamma_{ab}, \tag{3.65}$$

which is the evolution equation of the spatial metric. In our adopted coordinates these evolution equations can be written as

$$\begin{aligned} \mathcal{L}_t K_{ij} &= \beta^k \partial_k K_{ij} + K_{ki}\partial_i\beta^k + K_{kj}\partial_j\beta^k - D_i D_j \alpha && (3.66)\\ &+ \alpha(R_{ij} - 2K_{ik}K_j^k + KK_{ij}) + 4\pi\alpha(\gamma_{ij}(S-\rho) - 2S_{ij}), \\ \mathcal{L}_t \gamma_{ij} &= \beta^k\partial_k\gamma_{ij} + \gamma_{ki}\partial_i\beta^k + \gamma_{jk}\partial_j\beta^k - 2\alpha K_{ij} && (3.67) \end{aligned}$$

these are Arnowitt-Desner-Misner (ADM) $3+1$ formalism equations and together with the constraint equations (3.50)-(3.51), which form a Cauchy problem of the field equations in general relativity. We have managed to reduce the complexity of solving the Einstein field equations to solving these partial differential equations which are first order in time and second order in space.

3.5 Hyperbolicity and Well-Posedness

We can write the classification of the partial differential equations by considering different cases of the general second-order equation

$$A\partial_a^2 u + 2B\partial_a\partial_b u + C\partial_b^2 u = \hat{\rho}, \tag{3.68}$$

where A, B, C are real and smooth, and never vanish simultaneously. Hence we can obtain the different partial differential equations based on the conditions satisfied by the variables A, B, C [52] such that when

- $AC - B^2 < 0$, then we recover the *hyperbolic* equations.
- $AC - B^2 = 0$, this case gives us the *parabolic* equations through a simple coordinate change.
- $AC - B^2 > 0$, then we can recover the *elliptic* equations through a coordinate transformation that maps (a, b) to some region of the 3-d spacetime.

In the previous sections we have seen that the constraint equations take up the form of elliptic type PDEs, the ADM evolution equations are in hyperbolic, and the gauge conditions can be elliptic or parabolic depending on the spacetime slicing as we will see in section (3.7).

We now have the ADM evolution equations that we can use to evolve a generic spacetime given some initial data. In addition, we can use gauge conditions to specify the lapse function and shift vector. Although after a short moment of running the simulation, our code would crash due to due to small constraint violating errors getting amplified during evolution. In free evolution schemes, there is no way for the constraint to correct themselves while running the numerical simulation as they have satisfied every hypersurface up to that point, and continuing to do so on the current hypersurface even with the existence of the constraint violations. The constraint equations we have are elliptic equations, and some would correct the constraint violation by finding the solutions to these constraint equations, see [47].

Although following this approach is computationally expensive and requires more advanced techniques. The stability of these solutions is due to their well-posedness and hyperbolicity. To solve these equations, it has been found that well-posedness is an essential property that must be satisfied by the solutions. Alone it is not enough as some solutions are well-posed but not hyperbolic enough compared to others, this concept of Hyperbolicity is studied extensively in [48].

To understand these two concepts, let us consider a partial differential system of the form

$$\partial_t \boldsymbol{u} = \boldsymbol{P} \cdot \boldsymbol{u}, \tag{3.69}$$

where $\mathbf{u}$ is an n-dimensional solution vector function of time and space, and $\mathbf{P}$ is an $n \times n$ matrix with smooth spatial derivative operators as components. Given the solution at the zeroth hypersurface $\boldsymbol{u}(0, x)$, the problem is to solve this system for solutions $\boldsymbol{u}(t, x)$ at the successive hypersurfaces making this a Cauchy/initial value problem. Suppose we have a solution $\boldsymbol{u}(t, x)$ and changing the initial data $\boldsymbol{u}(0, x)$ even the slightest also changes the solution on every hypersurface $i.e$ the solution continually depends on the initial data. Mathematically the norm of the solution is bounded such that

$$||\boldsymbol{u}(t, x)|| \leq ke^{\alpha t}||\boldsymbol{u}(0, x)||, \tag{3.70}$$

for all hypersurfaces ($0 \leq t$), and the two constants k and α are independent of the initial data. When a solution cannot increase more rapidly than exponentially like we have described above, then the solution is called $well - posed$.

We look at partial differential equations in first order form that are said to be hyperbolic such that

$$\partial_t \boldsymbol{u} + \boldsymbol{A^i} \partial_i \boldsymbol{u} = \boldsymbol{S}, \tag{3.71}$$

where A^i are $n \times n$ matrices, $\boldsymbol{S} = \boldsymbol{S}(\boldsymbol{u})$ is a source vector and $i = 1, 2, 3$. If this system without the source vector is found to be a well-posed system this implies that a system where the source vector is linear in $\boldsymbol{u}$ is also well-posed. Therefore for the remainder of this section we assume there are no sources and set $\boldsymbol{S} = 0$. The hyperbolicity of the system is encoded into the matrix $\boldsymbol{A}$, let us assume that its components are constants and then define for an arbitrary unit vector n^i a matrix such that

$$\boldsymbol{P} = \boldsymbol{A^i} n_i, \tag{3.72}$$

and it is known as the *principal symbol* or the *characteristic matrix* of the system. Then based on the properties of the principal symbol, we have different notions of hyperbolicity such that the system is

- *strongly hyperbolic* if the principal symbol has real eigenvalues and a complete set of eigenvectors, for all n_i.
- *weakly hyperbolic* if the principal symbol has real eigenvalues but not a complete set of eigenvectors, for all n_i
- *symmetric hyperbolic* if the principal symbol can be symmetrized independently of the n^i

therefore systems that are symmetric hyperbolic are also strongly hyperbolic, but not all strongly hyperbolic systems are also symmetric hyperbolic. There are several ways other authors introduce hyperbolicity. Since our ADM equations are second order in space and first order in time, other ways is to derive the hyperbolicity of second order systems for example [49] and [50]. This intuitively tells us that strongly hyperbolic systems are well-posed and furthermore they have a finite speed of propagation of signals, more specifically in terms of the initial data they posses a finite past domain dependence. The ADM formulation has been shown to be weakly hyperbolic, which is responsible for its poor performance under numerical evolutions [43].

There are several alternate formulations of the ADM equations that lead to strongly hyperbolic equations that have been studied before under the initial value problem for Einstein's equations. One of them is known as the BSSNOK formulation which was first introduced by Oohara, Kojima,and Nakamura in [59], then later modified by Shibata and Nakamura in [51], it received an incredible amount of recognition from Baumgarte and Shapiro in [52] showing how stable it was compared to others, which we refer to as BSSNOK in this thesis to honour the original authors. Another well known and used formulation to run numerical simulations is the Z4-formulation which develops strongly hyperbolic system of equations from a covariant Lagrangian [53, 54]. In this thesis we will only recast the ADM equations in the BSSNOK formulation which we discuss further in the next section. As there are more formulations, that shows how most of these have their disadvantages which could be due to how one formulation introduces new variables that require more computational power for the new variable's equations or introducing inaccuracy through assuming vacuum to lessen the work of taking derivatives of the original equations while there may be matter present, refer to [55–58].

3.6 BSSNOK Formulation

To derive the BSSNOK formulation we consider first the new variable obtained from the inverse product of a conformal factor and the spatial metric such that

$$\bar{\gamma}_{ij} = \psi^{-4}\gamma_{ij}. \tag{3.73}$$

We fix ψ such that it relates to the determinant of the spatial metric in the way

$$\psi^4 = \gamma^{1/3} \tag{3.74}$$

where $\gamma = det(\gamma_{ij})$. This condition imposed on the conformal factor ensures that the determinant of the conformal metric to be unit $i.e\ \bar{\gamma} = 1$. It is convenient however to split the extrinsic curvature into its traceless part and trace such that

$$K_{ij} = A_{ij} - \frac{1}{3}\gamma_{ij}K, \tag{3.75}$$

and transform them individually, the re-scaled traceless extrinsic is obtained by

$$\bar{A}_{ij} = \psi^{-4}A_{ij}. \tag{3.76}$$

In the literature the usually adopted form of the conformal factor is

$$\psi = e^{\phi}, \tag{3.77}$$

since we require $\bar{\gamma} = 1$. An analytical solution for ϕ then follows as

$$\phi = \frac{1}{12}ln|\gamma|. \tag{3.78}$$

The conformal transformation for the spatial metric and the traceless extrinsic curvature are then given by

$$\bar{\gamma}_{ij} = e^{-4\phi}\gamma_{ij}, \tag{3.79}$$
$$\bar{A}_{ij} = e^{-4\phi}A_{ij}. \tag{3.80}$$

Now that we have introduced these new variables, we need to rewrite the ADM equations in terms of these variables. Let us consider the contracted evolution equations of (3.67) which is in terms of the determinant of the spatial metric

$$\partial_t\gamma = -2(\alpha K - \gamma\partial_i\beta^i) + \beta^i\partial_i\gamma. \tag{3.81}$$

Then we substitute the determinant of the conformally related spatial metric to find the evolution equation of the potential as

$$\partial_t\phi = \frac{1}{6}(\partial_i\beta^i - \alpha K) + \beta^i\partial_i\phi. \tag{3.82}$$

Following with the contracted evolution equation of the extrinsic curvature such that

$$\partial_t K = -\gamma^{ij}\nabla_j\nabla_i\alpha + \alpha(\bar{A}_{ij}\bar{A}^{ij} + \frac{1}{3}K^2) + 4\pi\alpha(\rho + S) + \beta^i\partial_i K. \tag{3.83}$$

We obtain the traceless evolution equations from subtracting the contracted equations from the equations (3.66) and (3.67). Also since we know that the trace-free part of a tensor X in our spacetime can be given by $X^{TF}_{ij} = X_{ij} - \gamma_{ij}X/3$, at the end which gives us the evolution equations in terms of (3.79) and (3.80) as

$$\partial_t \bar{\gamma}_{ij} = -2\alpha \bar{A}_{ij} + \beta^k \partial_k \bar{\gamma}_{ij} + \bar{\gamma}_{ik}\partial_j \beta^k + \bar{\gamma}_{kj}\partial_i \beta^k - \frac{2}{3}\bar{\gamma}_{ij}\partial_k \beta^k, \tag{3.84}$$

$$\begin{aligned} \partial_t \bar{A}_{ij} = e^{-4\phi}\big(- \bar{\nabla}_i \bar{\nabla}_j \alpha + \alpha(R_{ij} - 8\pi S_{ij})\big)^{TF} + \alpha(K\bar{A}_{ij} - 2\bar{A}_{ik}\bar{A}^k_j) \\ + \beta^k \partial_k \bar{A}_{ij} + \bar{A}_{ik}\partial_j \beta^k + \bar{A}_{kj}\partial_i \beta^k - \frac{2}{3}\bar{A}_{ij}\partial_k \beta^k. \end{aligned} \tag{3.85}$$

The superscript TF shows that the term is the trace-free part of a tensor and the extra terms in the Lie derivatives of both the variables along the shift vector, are due to the conformally related variables having a tensor density of weight $-2/3$.

In the evolution equation of $\bar{A}_{ij}$ there is a term involving the Ricci tensor. We can split it in terms of its dependence to the conformal factor such that

$$R_{ij} = \bar{R}_{ij} + R^{\phi}_{ij}, \tag{3.86}$$

where R^{ϕ}_{ij} in our adapted system can be rewritten as

$$R^{\phi}_{ij} = -2\bar{\nabla}_i \bar{\nabla}_j \phi - 2\bar{\gamma}_{ij}\bar{\nabla}^k \bar{\nabla}_k \phi + 4\bar{\nabla}_i \phi \bar{\nabla}_j \phi - 4\bar{\gamma}_{ij}\bar{\nabla}^k \phi \bar{\nabla}_k \phi. \tag{3.87}$$

Then the conformally related Ricci tensor is obtained by expressing the explicit form of the Ricci tensor in terms of the spatial metric as

$$\begin{aligned} R_{ij} = \frac{1}{2}\gamma^{kl}(\partial_i \partial_l \gamma_{kj} + \partial_k \partial_j \gamma_{il} - \partial_i \partial_j \gamma_{kl} - \partial_k \partial_l \gamma_{ij}) \\ + \gamma^{kl}(\Gamma^m_{il}\Gamma_{mkj} - \Gamma^m_{ij}\Gamma_{mkl}). \end{aligned} \tag{3.88}$$

Which contains the second derivatives of the spatial metric which is what we are trying to avoid from the field equations. Although before we substitute the conformally related metric we introduce conformal connection functions [52] such that

$$\bar{\Gamma}^i \equiv \bar{\gamma}^{jk}\bar{\Gamma}^i_{jk}. \tag{3.89}$$

These are the connection coefficients in terms of the conformally related spatial metric $\bar{\gamma}_{ij}$ and in Cartesian coordinates when $\bar{\gamma} = 1$, they take the form

$$\bar{\Gamma}^i = -\partial_k \bar{\gamma}^{ik}. \tag{3.90}$$

We then rewrite the Ricci tensor in terms of these conformal variables which gives us the conformally related Ricci tensor as

$$\bar{R}_{ij} = -\frac{1}{2}\bar{\gamma}^{lm}\partial_l \partial_m \bar{\gamma}_{ij} + \bar{\gamma}_{k(i}\partial_{j)}\bar{\Gamma}^k + \bar{\Gamma}^k \bar{\Gamma}_{(ij)k} + \bar{\gamma}^{kl}(\bar{\Gamma}^m_{il}\bar{\Gamma}_{mkj} - \bar{\Gamma}^m_{ij}\bar{\Gamma}_{mkl}). \tag{3.91}$$

We note that only the first term has second derivatives of the spatial metric. We then promote the conformally related connection functions to new independent functions of time, from one

hypersurface to the next such that they can then be evolved and their evolution equation is obtained by interchanging the spatial derivative with the time derivative of equation (3.90) which takes the form

$$\partial_t \bar{\Gamma}^i = -\partial_j \partial_t \bar{\gamma}_{ij}. \tag{3.92}$$

We can use the evolution equation of the conformally related spatial metric, to eliminate the second order derivative on the extrinsic curvature using the momentum constraint (3.50) and therefore the evolution equation for the conformal connection functions is obtained as

$$\begin{aligned} \partial_t \bar{\Gamma}^i = &-2\bar{A}^{ij}\partial_j \alpha + 2\alpha\big(\bar{\Gamma}^i_{jk}\bar{A}^{kj} - \frac{2}{3}\bar{\gamma^{ij}}\partial_j K - 8\pi\bar{\gamma}^{ij}S_j + 6\bar{A}^{ij}\partial_j\phi\big) \\ &+\beta^j\partial_j\bar{\Gamma}^i - \bar{\Gamma}^j\partial_j\beta^i + \frac{2}{3}\bar{\Gamma}^i\partial_j\beta^j + \frac{1}{3}\bar{\gamma}^{li}\partial_l\partial_j\beta^j + \bar{\gamma}^{lj}\partial_j\partial_l\beta^i. \end{aligned} \tag{3.93}$$

To take a step back and recap what we have done in this section, we have simply reduced the order in space to first order. From the weakly-hyperbolic ADM equations we conformally transformed its variables and introduced more variables $\{\phi, K, \bar{\gamma}_{ij}, \bar{A}, \bar{\Gamma}^i\}$ along with their evolution equations are (3.82)−(3.85), and (3.93). This is the new system of evolution for our spacetime which was proven empirically to be far more stable than the ADM by [52].

As we have mentioned that the ADM equations are weakly-hyperbolic, and it turns out these BSSNOK equations are strongly-hyperbolic, this has been proven in depth by Sarbach *et. al* in [60] where they developed an equivalence between this formalism and other strongly/symmetric hyperbolic formalism, and they achieved this from mapping them to the Kidder–Scheel–Teukolsky evolution equations [61]. Furthermore we can obtain symmetric hyperbolic systems from these equations [60, 62].

3.7 Gauge Conditions

The field equations do not provide any evolution equations for the lapse α and shift β^i, a fact related to the coordinate freedom inherent in the theory. To close either the ADM or BSSN system, we need a way to specify the gauge functions. The process behind choosing these conditions is left to knowing what the hypersurfaces should be shaped like when evolved through spacetime and that their spatial coordinates are physical. In [43] they provided an elaborate outline of the desired results such that the gauge conditions should: avoid any appearance of singularities, both coordinate and physical singularities; be easy to implement, leading to well-behaved evolution equations; be setup such a way that we can choose a co-rotating coordinate system to 'exploit' the symmetry of of the system to our advantage; be in 3-covariant form to allow them to be invariant under coordinate change.

3.7.1 Geodesic Slicing

This is the simplest gauge condition where we require that our Eulerian observer - travelling through the unit normal vector - measures the same proper time interval travelled as the non-Eulerian observers such that

$$d\tau = dt.$$

It follows that this leads to a constant lapse function as

$$\alpha = 1. \tag{3.94}$$

Additionally we require that our Eulerian observer coincide with the non-Eulerian observer such that

$$x^i(t + dt) = x^i(t),$$

and this translates to imposing a vanishing shift vector

$$\beta^i = 0. \tag{3.95}$$

This is considered a prescribed slicing condition. It derives its name from the free-falling Eulerian observers since their lapse function is unit, that leads to a vanishing acceleration from equation (3.4), and this turn their worldlines into timelike geodesics.

We apply this condition on the evolution equation of the trace of the extrinsic curvature in (3.83) we find that it reduces to

$$\partial_t K = K_{ij}K^{ij} + 4\pi(\rho + S). \tag{3.96}$$

Recall that $K_{ij}K^{ij} \geq 0$, additionally according to the strong energy conditions [64], the second term also satisfies $(\rho + S) \geq 0$. Thus the expansion of our Eulerian observer monotonically decreases along their timelike geodesic, this implies that the trace of the extrinsic curvature monotonically increases without any boundary from hypersurface to the next *i.e* hypersurfaces warps more as we are moving along the geodesic. This gauge condition affects the spatial metric through the contracted evolution equation (3.81) such that it reduces to

$$\partial_t ln\gamma^{1/2} = -K. \tag{3.97}$$

Since $\gamma^{1/2}d^3x$ measures the coordinate volume element that is swept up by the warping hypersurface as it moves along the geodesic, the above equation shows that the volume decreases monotonically. This is not a good property for the evolution, as this would result in a cone like spacetime with a coordinate singularity. The implications of a coordinate singularity to observers free-falling in geodesics through a non-uniform gravitational field, is that these observers could end up being pulled towards each other and occupy the same point with different set of coordinates in our spacetime by the nature of geodesics. This makes the geodesic slicing condition the least favorite gauge condition.

3.7.2 Maximal Slicing

As the the previous gauge condition converges to a singularity, we are compelled to further look for a better choice keeping in mind the desired results of our foliated spacetime. We can start by looking at how the geodesic condition failed and try to rectify that in the new condition. That would mean that we could look at how we can impose boundaries on how much the mean curvature K can evolve. This further translates into imposing boundaries on the coordinate volume elements of our free-falling Eulerian observers, instead of them decreasing monotonically we could demand that they remain constant, this is implicit singularity avoidance. To build up to this condition, let us first assume that the mean curvature is a function of both space and

time, this makes the evolution equation (3.66) becomes an elliptic function in terms of the lapse function such that

$$D^i D_i \alpha = -\partial_t K + \alpha(K_{ij}K^{ij} + 4\pi(\rho + S)) + \beta^i D_i K. \tag{3.98}$$

Going back to demanding the mean curvature to remain constant, and the maximal slicing condition chooses

$$K = 0. \tag{3.99}$$

We do not only impose this condition on the initial hypersurface but throughout all times, then the change of the coordinate volume elements remains constant such that

$$\partial_t K = 0. \tag{3.100}$$

This condition simplifies the elliptic equation for the lapse function we have encountered to a condition for the lapse function to satisfy in on each hypersurface

$$D^i D_i \alpha = \alpha(K_{ij}K^{ij} + 4\pi(\rho + S)). \tag{3.101}$$

We notice how the shift vector term vanishes in our evolution equation, hence the maximal condition additionally decouples the lapse function and shift vector conditions. The condition derives its name from the property of ensuring that every slice in our spacetime is maximal with a Von Neumann condition along its boundaries. This property was shown in [65] by considering very small deformations along a vector around the coordinate volume elements $vol(S)$ around a portion S of an hypersurface, we know that $vol(S) = \int_S \gamma^{1/2} d^3x$. The variation of these volume elements vanishes due to their dependence on the mean curvature $i.e\ \delta vol(S) = 0$. Although if the signature of our spacetime metric g_{ab} were a form of Euclidean geometry, we would be presented with hypersurfaces that deformed to their minimal slices ***i.e Plateau's Problem [66].***

3.7.3 Harmonic Slicing

In the previous slicing condition we had to evaluate an elliptic equation of the lapse function at each hypersurface to foliate spacetime, this is computationally expensive and furthermore its gets more costly in 3-d. It is possible to develop an easier to implement condition that approximates the system to maximal slicing with hyperbolic equations and still provides a stable spacetime. We take the approach of requiring the coordinate x^a to satisfy the wave equation

$$\Box x^i = 0. \tag{3.102}$$

This condition simplifies the Einstein's field equation impeccably, and presents them as a series of nonlinear wave equations that can be proven to have maximal foliation and stability [67]. We can expand the harmonic condition such that

$$g^{ab}\nabla_a \nabla_b x^i = 0. \tag{3.103}$$

The contraction of the connection symbols with the 4-metric allows us to rewrite equation (3.102) such that

$$g^{ab}\Gamma^c_{ab} \;=\; -\frac{1}{g^{1/2}}\partial_b(|g|^{1/2}g^{ab}), \tag{3.104}$$

which implies that

$$\partial_b(|g|^{1/2}g^{ab}) = 0. \tag{3.105}$$

This is the *Harmonic slicing* condition, and we recall that we have the explicit form of the inverse 4-metric on (3.16) which gives the coupled, non-linear and hyperbolic equations of the lapse function and shift vector as

$$(\partial_t - \beta^i\partial_i)\alpha = -\alpha^2 K, \tag{3.106}$$

$$(\partial_t - \beta^i\partial_i)\beta^j = -\alpha^2(\gamma^{ij}\partial_j ln\alpha + \gamma^{jk}\Gamma^i_{jk}). \tag{3.107}$$

Now this condition has promoted the lapse function and shift vector to dynamic variables that require time evolution in our spacetime, although these are hyperbolic equations which are easier to solve compared to the elliptic equation in the last section.

3.7.4 Bona-Masso Slicing

This work on the harmonic-slicing has led to the development of the hyperbolic form of equations for the lapse function that mimicked the maximal slicing conditions and furthermore are singularity avoiding by Bona and Masso [68] where it was proved that the harmonic slicing only avoided the singularity up to a certain point, and it was unmatched compared to the maximal slicing that avoided stronger singularities due to its collapsing lapse function when approaching a singularity. The extensive work of Bona and Masso on the vacuum Einstein field equations in the harmonic slicing gauge [69–71] has led to the development of a class of generalised slicing conditions called the *Bona-Masso* family of slicing condition [72], such that the lapse function satisfies the evolution equation

$$(\partial_t - \beta^i\partial_i)\alpha = -\alpha^2 f(\alpha)K, \tag{3.108}$$

where $f(\alpha)$ is an arbitrary positive function of α only. We are able to recover numerous slicing conditions from the behavior of the function $f(\alpha)$, such that in the case $f = 0$ and $\alpha = 1$ we obtain the *geodesic slicing* condition (3.94). While the case $f = 1$ corresponds to the harmonic slicing condition (3.106). Although in the case of a diverging function $i.e\, f(\alpha) \to \infty$, the condition behaves like the *maximally slicing* condition [63], and we recover the strong singularity avoidance. One other interesting algebraic condition that can be recovered is the $1 + log$ slicing condition when $f = 2/\alpha$, and with a vanishing shift vector we can integrate equation (3.108) to obtain

$$\alpha = 1 + log\gamma, \tag{3.109}$$

by choosing the constant of integration to be unity. The $1 + log$ slicing condition is one of the stable and robust algebraic conditions that has proven to be very effective when evolving black holes in 3-d [73] and also strong gravitational fields [74].

3.8 Matter Equations

In nonvacuum relativistic spacetimes we have all kinds of matter sources that need to be considered when evolving our system. We then have to understand their equations of motion in response to the changing geometry of spacetime. The motion of the relativistic fluid has to satisfy the laws of thermodynamics in the spacetime. In addition, also most importantly the law of

local conservation of energy-momentum (2.15) in the isolated system. Which in the covariant form these conservation laws are

$$\nabla_a T^{ab} = 0, \tag{3.110}$$

and along with the conservation of the rest-mass

$$\nabla_a (\rho u^a) = 0. \tag{3.111}$$

From here let us assume that our fluid has no heat conductivity and furthermore there are no viscosity effects present between its infinitesimal elements, such a fluid is said to be a *perfect fluid*. The stress-energy tensor of a perfect fluid is given by

$$T_{ab} = \rho_0 h u_a u_b + p g_{ab}. \tag{3.112}$$

As before the four velocity of the fluid elements is denoted by u^a, where ρ_0 and p denoted their rest mass-energy density measured in the fluid's rest frame and their pressure respectively. The quantity h is the fluid's specific enthalpy which is given by

$$h := 1 + \epsilon + \frac{p}{\rho_0}, \tag{3.113}$$

where the quantity ϵ is the specific internal energy density, which gives us the total energy density of the fluid when summed with the rest-mass energy which is obtained by

$$\rho = \rho_0 (1 + \epsilon). \tag{3.114}$$

To obtain the equations of motion now from the conservation laws, we present different approaches that introduce different variables to cast the equations in various suited forms for numerical integration.

3.8.1 High-Resolution Shock-Capturing Schemes

The hydrodynamic formulation will require us to first cast the covariant conservation equations (2.15), (3.111) into a first order hyperbolic system of flux conservation equations of the form

$$\partial_t \mathcal{U} + \partial_i \mathcal{F}^i = \mathcal{S}. \tag{3.115}$$

The vector $\mathcal{U}$ is called the state vector of the conserved variables in the system in terms of the primitive variables (ρ_0, ϵ, v^i) is given [81] as

$$\mathcal{U} = \begin{bmatrix} \tilde{D} \\ \tilde{S}_i \\ \tilde{\tau} \end{bmatrix} = \sqrt{\gamma} \begin{bmatrix} W\rho_0 \\ \alpha\sqrt{\gamma} T^0_j \\ \alpha^2 \sqrt{\gamma} T^{00} - \tilde{D} \end{bmatrix}, \tag{3.116}$$

where $W = -n^a u_a$ is the Lorentz factor which satisfies

$$W = (1 - v^i v_i)^{-1/2}, \tag{3.117}$$

We obtain the flux vector $\mathcal{F}^i$ as

$$\mathcal{F}^i = \begin{bmatrix} \tilde{D} v^i \\ \alpha\sqrt{\gamma} T^i_j \\ \alpha^2 \sqrt{\gamma} T^{0i} - \tilde{D} v^i \end{bmatrix} \tag{3.118}$$

and the source vector $\mathcal{S}$ becomes

$$\mathcal{S} = \sqrt{\gamma} \begin{bmatrix} 0 \\ \frac{1}{2}\alpha T^{ab}\partial_i g_{ab} \\ \alpha T^{0a}\partial_a \alpha - \Gamma^0_{ab} T^{ab}\alpha \end{bmatrix}. \tag{3.119}$$

The key feature that makes these equations shock-capturing is that the sources equations do not include any gradients of the primitive variables, these equation do not break the nature of the hyperbolic system. Now one needs to understand the characteristic fields and speeds of the system by computing the eigenvalues and eigenvectors of the Jacobian matrix

$$\frac{\partial F^i}{\partial \mathcal{U}}. \tag{3.120}$$

Finally, we present the fluid's contribution to the source terms of the system from the projections of the stress-energy tensor of the perfect fluid measured by our Eulerian observer

$$\begin{aligned}
\rho &= n_a n_b T^{ab} && (3.121)\\
&= \rho_0 h W^2 - p, && (3.122)\\
S_i &= -\gamma_{ia} n_b T_{ab} && (3.123)\\
&= \rho_0 h W u_i, && (3.124)\\
S_{ij} &= \gamma_{ia}\gamma_{jb} T^{ab} && (3.125)\\
&= p\gamma_{ij} + \frac{S_i S_j}{\rho_0 h W^2}, && (3.126)\\
S &= \gamma^{ij} S_{ij} && (3.127)\\
&= 3P + \rho_0 h (W^2 - 1), && (3.128)
\end{aligned}$$

where in the Eulerian frame the Lorentz factor satisfies $W = (1 + u^i u_j)^{1/2}$.

Chapter 4

Numerical Methods

In the previous chapters we have derived the evolution equations that are in partial differential forms. Solving these equations numerically is the vast basis area of numerical relativity. These equations are in partial differential form in terms of both space and time in most cases, and that alone makes them more complex than ordinary differential equations to solve exactly. Furthermore, they get more challenging to solve when they have features such as higher order spatial derivatives, non-linearities in the variables and/or discontinuities. These challenges are what have led to the vast approximate numerical schemes that have been developed for decades to handle all the intricate cases of partial differential equations (PDE).

The thematic problems in this thesis are hyperbolic in nature. As a result, we restrict our treatment in this chapter to methods for hyperbolic PDEs. Therefore in this chapter, we will discuss the introduction concepts to some widely used methods to solve PDEs, we will first cover basic finite differencing methods and then some high order methods.

4.1 Finite-Difference Methods

In order to solve a PDE of the function $u(t, x^i)$ in our continuous spacetime, we require to know its value for each point in space and time. This presents us with an infinite amount of values to cover the hypersurface at all times. These are all unknown variables of the functions. The method of finite differencing considers reducing the domain of dependence of the function to a finite set of points in spacetime. The discretized spacetime is called a *grid* with discrete points (t^n, x_i) - these are not to be confused with the elements vectors we have worked with thus far - that are separated by grid spacing that can be uniform throughout the entire grid or nonuniform, depending on the method used. The grid spacings are denoted by Δt for two hypersurfaces and Δx for two adjoining spatial points. To make the discretization uniform the grid spacings can be set as constant by

$$x_i = x_0 + i\Delta x, \tag{4.1}$$

along with the time step

$$t^n = t^0 + i\Delta t. \tag{4.2}$$

The function has now finite discrete values on the grid and we use the grid points to denote as

$$u_i^n = u(t^n, x_i) + error, \tag{4.3}$$

where the truncation error is introduced by the convergence of the finite difference solution to differential equation solution. The truncation error should approach zero as the step-sizes Δt and Δx approach 0, see for example [43, 82]. We suppose that the function u is sufficiently differentiable. This then allows us to Taylor expand the function u at a point x_{i+1} about x_i for constant time level such that

$$u_{i+1} = u(x_i + \Delta x) = u(x_i) + \Delta x(u_x)_i + \frac{(u_x^2)_i}{2!}(\Delta x)^2 + \mathcal{O}(\Delta x^3), \tag{4.4}$$

where the i around the partial derivatives denotes the evaluation of the derivatives at the point x_i. With the higher order terms considered negligible then the partial derivative of the function is obtained by

$$(u_x)_i = \frac{u_{i+1} - u_i}{\Delta x} + \mathcal{O}(\Delta x), \tag{4.5}$$

where the linear truncation error is the result of dividing by Δx. Similarly, a Taylor expansion of $u(x - \Delta x)$ yields

$$u_{i-1} = u(x_i - \Delta x) = u(x_i) - \Delta x(u_x)_i + \frac{(u_x^2)_i}{2!}(\Delta x)^2 + \mathcal{O}(\Delta x^3). \tag{4.6}$$

If these two equations (4.4) and (4.6) are subtracted and solved for the first order partial derivative, we then get

$$(u_x)_i = \frac{u_{i+1} - u_{i-1}}{2\Delta x} + \mathcal{O}(\Delta x^2), \tag{4.7}$$

noting that this representation of the first order partial derivative has a low truncation error which is quadratic compared to the first one we derived at (4.5).

We use the same equations (4.4) and (4.6), but now we add them to obtain the representation second-order derivative and divide by the quadratic term of the grid spacing to obtain

$$(u_x^2)_i = \frac{u_{i+1} - 2u_i + u_{i-1}}{(\Delta x)^2} + \mathcal{O}(\Delta x^2). \tag{4.8}$$

We have the finite-difference representation of the function u in the grid space along with its first two derivatives, we can obtain higher than second-order derivatives in space and time by carrying the similar derivation. We are now in the position to rewrite any partial derivative problem in terms of the finite-difference derivatives and solve for the solution. The fundamental requirement in numerical relativity when solving systems is the existence of a unique solution of convergence and the generation of stable solutions. Although in order to be in the position to discuss these concepts we require the notion of the norm of the finite-difference solutions in analogous to the true solution's. We introduce the discretized p-norm of the smooth function $u(t, x^i)$ in the spatial region Σ as

$$||u||_p = \left(\frac{1}{(b-a)}\int_\Sigma |u(t, x^i)|^p dx^i\right)^{1/p}. \tag{4.9}$$

And we can extend this to include the time dependency of the finite difference function such that

$$||u(t^n)||_p = \left(\frac{1}{J}\Sigma_{i=0}^J |u_i^n|^p\right)^{1/p}, \tag{4.10}$$

where J is the total number of grid points. The case when $p = 2$ results in the 2-norm equation as the root mean square equation used to measure the mean of the finite difference solution form all its discrete values on our specified grid. Then now we can look at the fundamental requirements of the scheme. For stability we recall the well-posedness condition (3.70), and then here the stability condition is the discrete version of it such that, the grid is considered to be stable if we can find real constants K and σ that satisfies the bound

$$||u(t,\cdot)||_q \leq Ke^{\sigma t^n}||u(0,\cdot)||_q, \tag{4.11}$$

which guarantees that when the grid spacings $\Delta x, \Delta t$ approaches zero (*i.e p → 0*), the solutions are then bounded [83] for all of t_n. Although for the approximated solutions to entail the properties of the original differential equation, the solutions are required to be consistent. For a discretization to be consistent the error must satisfy the limit

$$\lim_{q\to 0} ||u^n - u(t_n,\cdot)||_q = 0. \tag{4.12}$$

With both of these notions (*stability and consistency*) assumed to hold our finite difference scheme, we can further conclude that our discretization is u_i^n converges to the true solution $u(t, x^i)$. In appendix (B), we apply these concepts on the hyperbolic systems of PDEs we have introduced at the beginning of this chapter introductory in depth.

4.2 Method of Lines

We present here one of the most widely used numerical method to discretize both hyperbolic and parabolic differential equations, as it serves as an alternative to the finite-differencing schemes we have presented and mentioned in the previous section. The previous methods treated discretizing both time and space dimensions at same level. This approach makes it harder to achieve higher-order accuracy for time. Treating them distinctly is the basis of the method of lines (MOL). Numerically the basic idea behind the method of lines is such that for a partial differential equation in both time and space, one discretizes the spatial dimensions into grid points as we have seen previously, while the time dimension is left to be continuous. This converts the partial differential problem for u(t, x) into a semi-discrete problem of ordinary differential equations with a continuous time for the grid functions $u(t)_i$. We can then use any ODE solver to integrate the resulting systems of differential equations.

We illustrate the method of lines on the following model problem

$$\partial_t u + \partial_x F(u) = S(u) + \frac{1}{\tau}R(u), \tag{4.13}$$

where $S(u)$ is some source vector, and $R(u)$ is a vector that contains the *stiff* terms of the system with τ being the systems *relaxation time*. In the limit $\tau \to \infty$ the stiff terms vanish and the equation (4.13) represents a hyperbolic system in conservative form. The stiff terms are introduced into the system when it evolves over two different time-scales, which we will formally introduce in the next sections. Using the finite-difference scheme to discretize our spatial domain of dependence while leaving the time dimension continuous, promotes the system into a *semi-discrete* system of ordinary differential equations such that

$$\frac{d}{dt}u_i = Q(u_i) + \frac{1}{\tau}R(u_i). \tag{4.14}$$

With the advantage of decoupling the discretization of space and time, the method of lines aids greatly in codes that treat different systems. For example, when simulating neutron star dynamics, one needs to solve the wavelike BSSN equations coupled to the conservative hydrodynamic equations. In the next sections we will discuss different approaches to obtain the solutions to the semi-discrete system by the use of Runge-Kutta methods depending on whether the system contains stiff terms or not.

4.2.1 Explicit Runge-Kutta Methods

In the absence of the stiff term $\frac{1}{\tau}R(u)$ in the system, the model problem (4.13) becomes

$$\partial_t u - \partial_x F(u) = S(u). \tag{4.15}$$

We introduce a spatial grid that promotes our continuous functions $u(t,x)$ to semi-discrete functions $u(t,x_i) = u(t)_i = u_i$ that are still continuous functions of time in our spatial grid.

The Method of Lines or the discretization methods discussed in section (4.1) can be used to recast the problem (4.15) into an ordinary differential equation of the form

$$\frac{du}{dt} = Q(u). \tag{4.16}$$

The time integration can be handled via explicit Runge-Kutta methods, which were first introduced as less computationally expensive generalization to the Taylor's method to solve ODEs. Runge introduced them in [88] and half a decade later Kutta reformulated them in [89]. A second order Runge-Kutta method for the system (4.16) yields

$$u^{n+1} = u^n + \Delta t Q(u^*), \tag{4.17}$$

$$u^* = u^n + \frac{\Delta t}{2} Q(u^n). \tag{4.18}$$

Which calculates the solutions for the next time step using the current time step to find the intermediate values u^* to advance the solution half a time step using the midpoint method. These intermediate values are used to obtain the time independent sources at half a time step to calculate the next solution and fully advance the time step.

This scheme is referred to as MOL-RK2 with a local truncation error of $\mathcal{O}(h^2)$. The time step still has to satisfy the *Courant-Friedrichs-Lewy* (CFL) condition, which is a necessary relation of the time step to the spatial step up to a constant guaranteeing convergence [85, 86]. Although we can use a superior stable Runge-Kutta method [90] with a local truncation error of $\mathcal{O}(h^4)$. For example, adopting the classic fourth order accurate method, the update formula become

$$u_i^{n+1} = u_i^n + \frac{\Delta t}{6}(k_1 + 2k_2 + 2k_3 + k_4), \tag{4.19}$$

where the intermediate stages k_i are computed from (4.16) as

$$k_1 = Q(u_i^n), \tag{4.20}$$

$$k_2 = Q(u_i^n + k_1 \Delta t/2), \tag{4.21}$$

$$k_3 = Q(u_i^n + k_2 \Delta t/2), \tag{4.22}$$

$$k_4 = Q(u_i^n + k_3 \Delta t), \tag{4.23}$$

which we refer to as the MOL-RK4 method. This method often is preferred due to its higher order accuracy and stability properties for non-stiff problems [91, 98].

The equations in (4.20)-(4.23) can be conveniently represented in the form of a Butcher table. Within this representation, the RK4 method becomes

$$\begin{array}{c|cccc} 0 & 0 & 0 & 0 & 0 \\ \frac{1}{2} & \frac{1}{2} & 0 & 0 & 0 \\ \frac{1}{2} & 0 & \frac{1}{2} & 0 & 0 \\ 1 & 0 & 0 & 1 & 0 \\ \hline & \frac{1}{6} & \frac{1}{3} & \frac{1}{3} & \frac{1}{6} \end{array}$$

The classic RK4 method is not suited for problems with stiff terms since one is restricted to using the smallest step size required to resolve all the scales of the problem. Most often though, RK methods with adaptive step sizes are used in this case. For their ability to maintain the local truncation error within bounds. Popular examples in this category are the Runge-Kutta-Fehlberg RK45 [92], Cash-Karp [93] and Dormand-Prince DOPRI methods [94]. These methods work by using an embedded pair of RK methods of differing order to enable error estimation and control [95, 98]. Suppose u^{n+1} and $\hat{u}^{n+1}$ are both approximation solutions obtained by RK pair of order $(m+1)$ and m respectively, then the quantity

$$\mu \leq \left(\frac{\varepsilon \Delta t}{|\hat{u}^{n+1} - u^{n+1}|} \right)^{1/n}, \tag{4.24}$$

with $\varepsilon > 0.$ is used to accept or reject the solution as follows

- if $\mu < 1$, reject the solution and recalculate with step size $\mu \Delta t$,
- if $\mu \geq 1$, accept the solution and update the step size to $\mu \Delta t$ for the next step's solution.

4.2.2 Implicit-Explicit Runge-Kutta Methods

While adaptive methods may be optimal compared to non-adaptive RK methods, function evaluations are wasted when steps are rejected. In addition, frequent step size adjustments may lead to loss of smoothness in the solution [102, 105]. An alternative is fully implicit schemes [102, 106]. However these also waste function evaluations in the solution of the resulting non-linear systems.

An efficient method for problems where the stiff components are easily separated, as in the model problem (4.13), is IMEX schemes. The explicit methods we have presented in the previous chapter do not usually work for these kinds of systems, then it becomes economical to use an explicit method to solve the non-stiff part and an implicit method for the stiff parts. Although before we jump into solving, let us formally introduce the concept of stiff differential equations. The system of ordinary differential equations of the form

$$\frac{du}{dt} = \hat{Q}(u), \tag{4.25}$$

where $\hat{Q}$ is the derivative operator containing the stiff and non-stiff terms. Stiff systems' definition came after it was shown that the use of the explicit methods to solve the system introduced

stability problems and the resulting system became unstable due to the inconsistency in their step size control [99]. We formally define the stiffness of the system (4.25) by considering a perturbed solution of the exact solution such that

$$u(t) \rightarrow u(t) + \delta u(t),$$

then our perturbed differential problem becomes

$$\frac{du}{dt} + \frac{d\delta u}{dt} = \hat{Q}(u + \delta u), \tag{4.26}$$

where the right-hand side is Taylor expanded around the exact solution of the original ODE and we neglect the higher order terms which gives

$$\hat{Q}(u + \delta u) \approx \hat{Q}(u) + \frac{\partial \hat{Q}}{\partial u}\delta u. \tag{4.27}$$

Then when substituting (4.27) in (4.26) we obtain the differential equation of the perturbation as

$$\frac{d\delta u}{dt} = \frac{\partial \hat{Q}}{\partial u}\delta u, \tag{4.28}$$

which tells us about how the perturbations change as time moves forward. Notice that if we keep the exact solution $u(t)$ and the Jacobian $\frac{\partial \hat{Q}}{\partial u}$ constant, then the change in the perturbations will depend on the eigenvalues of the Jacobian. Therefore, the problem becomes stiff if there exists one or more eigenvalues of the Jacobian denoted as λ_i, whose absolute real part is very negatively large [96] *i.e*

$$1 \ll \frac{max\{Re(\lambda_i)\}}{min\{Re(\lambda_i)\}}. \tag{4.29}$$

This introduces solutions that exhibits fast and slow dynamics. The concept of stiff differential problems appears on a range of other problems. One example is in chemical reaction systems when a system seem to have both fast and slow reactions; or in electrical circuits where the stiffness of the Van der Pol equation is controlled by its equation parameter; and in hyperbolic systems showing up as diffusion terms with relaxation times, this is the problem we are interested in solving in this thesis. As we have mentioned, that solving stiff equations with explicit methods introduces instability. This then prompts one to use implicit methods to solve them although these come with a disadvantage of requiring more evaluations per step than explicit methods. Other methods have been developed to solve the differential equations by employing a simple technique that checks for stiffness in a system and when it is detected, the code switches to an implicit method.

We now return to our model problem

$$\partial_t u = Q(u) + \frac{1}{\tau}R(u), \tag{4.30}$$

with τ as the stiffness parameter. We solve this system using the Implicit-Explicit Runge-Kutta (IMEX-RK) scheme. The basis of the IMEX-RK is based on splitting the stiff and non-stiff terms and solve them using implicit and explicit methods respectively by approximating their integration over a discrete temporal grid using an appropriate Runge Kutta formula. When

solving the hyperbolic system (4.30) we first use the method of separation on the system's terms into $u = \{f, g\}$ such that f and g denotes the system's stiff and non-stiff terms respectively, such that our split system of differential equations is

$$\partial_t f = Q_f(f, g), \tag{4.31}$$
$$\partial_t g = Q_g(f, g) + R_g(f, g). \tag{4.32}$$

And the non-stiff operator acts on the variables independently such that $Q = \{Q_f, Q_g\}$ and they each act on the variables with derivatives along the stiff and non-stiff terms respectively, and on the other hand the stiff operator only acts on the stiff terms with derivatives such that $R = \{0, R_g\}$. Then solving this system requires an explicit method applied on the non-stiff part (4.31) and using an implicit method to solve the stiff part (4.32).

The order conditions for an IMEX-RK scheme are determined by the accuracy of the numerical solution obtained at some time step compared to the true solution evaluated at the same time point. If the two solutions agree up a order $\mathcal{O}(\Delta t^{\eta+1})$ then the IMEX-RK scheme is said to be of order η with σ stages for the explicit scheme, and α stage for the implicit scheme. The IMEX-RK schemes are efficient for up to 3rd order which is considered higher order for these methods. The inaccuracy of these methods increase as one goes further than 4th order due to the coupling of the explicit and implicit scheme which makes them inefficient [103].

IMEX-RK schemes are further represented by the strong stability preserving (SSP) property such that up to 3rd order they maintain the strong stability of their discrete solutions while achieving high accuracy. Their representation is denoted by $SSP(\alpha, \sigma, \eta)$. The IMEX scheme we employ in this thesis is given by the following Butcher tableau

$$\begin{array}{c|ccc} 0 & 0 & 0 & 0 \\ \frac{1}{2} & \frac{1}{2} & 0 & 0 \\ 1 & \frac{1}{2} & \frac{1}{2} & 0 \\ \hline & \frac{1}{3} & \frac{1}{3} & \frac{1}{3} \end{array} \qquad \begin{array}{c|ccc} \frac{1}{4} & \frac{1}{4} & 0 & 0 \\ \frac{1}{4} & 0 & \frac{1}{4} & 0 \\ 1 & \frac{1}{3} & \frac{1}{3} & \frac{1}{3} \\ \hline & \frac{1}{3} & \frac{1}{3} & \frac{1}{3} \end{array}$$

denoted by SSP(3,3,2) from the explicit (left) and implicit (right) methods.

4.3 High Resolution Methods

When simulating fluid flows, there is always the potential that shocks will appear during the evolution. These shocks in the flow usually translate as discontinuities in the flow's solution. Inevitably the solution develops oscillations around the discontinuity causing it to break its local monotone property between two grid points. The scheme that leads to a general update statement such as

$$u_j^{n+1} = F(u_{j\pm1}^n, u_{j\pm2}^n, ..., u_{j\pm1}^{n+m}, u_{j\pm2}^{n+m} ...), \tag{4.33}$$

is said to be a monotone scheme when its Jacobian satisfies

$$\frac{\partial F}{\partial u_j^n} \geq 0, \tag{4.34}$$

for all the values u_j^n for both time and spatial grids. These schemes ensure that there is no local extrema that occurs in the flow of the solution with some enforcing a monotonicity constraint in the evaluation of the scheme. Furthermore a monotone scheme with

$$u_j^n \geq u_{j+1}^n, \tag{4.35}$$

is considered to be monotonicity preserving if it satisfies

$$u_j^{n+1} \geq u_{j+1}^{n+1} \tag{4.36}$$

for all values of n and j. This property ensures monotonicity throughout the time levels and avoids any change leading spurious significant increase in the solutions. These oscillations of the solution near the discontinuity can be measured in terms of their *total variation* (TV) property such that for a scheme (4.33) the magnitudes of oscillations can be inferred from

$$TV(u^n) = \sum_{-\infty}^{+\infty} |u_j^n - u_{j-1}^n|. \tag{4.37}$$

This property is further extended to define *total variation diminishing* (TVD) that can be used continuously in schemes to reduce the oscillations in the scheme by avoiding any increase in the total variation. A scheme is said to be TVD if it continuously satisfies

$$TV(u^{n+1}) \leq TV(u^n). \tag{4.38}$$

One of the drawbacks of TVD schemes is that they reduce to first order when they encounter a local extrema [44]. These concepts were unified by Harten [105] by showing that a monotone scheme is also total variation diminishing. In addition, a total variation diminishing scheme is monotonicity preserving.
The numerical methods that have pioneered treating discontinuities by building on these above fundamental properties for the flow of the solution are at most second order, we will just give an overview of them in this thesis. The first method is that which we have seen in the previous chapter 4.2, introduced by von Neumann and Richtmyer [78] is the addition of an artificial-viscosity that is meant to absorb the oscillatory effects of the discontinuity by extending them over some grids but negligible at the smooth flow. This method is simple enough to implement although, with the point of discontinuity extended over some grids, this method requires grid refinement to ensure that the shocks are not missed by the method. Now modern methods employ an adaptive grid refinement technique along with the method to adjust to the structures in the flow of the solution. This becomes more complex with more dimensions in the flow and hence slowing down the computation.

Another relevant method in this context is *Godunov's* method [106], which is part of the upwind methods. Godunov showed that higher than second order linear schemes are not oscillation free near discontinuities. Instead treated the problem as a nonlinear Riemann's shock tube problem since at a point of discontinuity x_j, the numerical solution was in different states from the left $x_{j-\frac{1}{2}}$ and right $x_{j+\frac{1}{2}}$. Therefore obtaining the solution through piercing discontinuous numerical solutions and generating a local Riemann problems in the grid such that

$$u(x,0) = \begin{cases} u_j^n & x < x_{j+\frac{1}{2}}, \\ u_{j+1}^n & x > x_{j+\frac{1}{2}}, \end{cases} \tag{4.39}$$

where the numerical values u_j^n represent the volume average in the cell $[x_{j+\frac{1}{2}}, x_{j-\frac{1}{2}}]$. This produces two nonlinear waves that can be rarefaction waves that propagate with a shock between them. This has proven to be a quite efficient method to use when treating conservative problems with discontinuities which heavily relies on the Riemann solver that governs the interaction between the two states. Riemann solver performs well near discontinuities than at the points of smooth flow, which comes with numerical dissipation in these smooth regions and hence a finer grid is often required.

While Godunov's method was only limited to linear and monotonicity preserving first order schemes, modern methods found that a higher order scheme can also be achieved by making the scheme nonlinear. In addition, instead of considering constant left and right states for the Riemann problem, the states are obtained by the use of *reconstruction* techniques to reconstruct higher order interpolation polynomials that describe the flow of the solution inside each grid cell based on the averages u_j^n. Numerous methods based on Godunov's approach have been developed such as the MUSCL scheme by Leer [107] which achieves second order accuracy by instead considering linear u_j^n states, and also the PPM scheme by Colella and Woodward [108] which is a piecewise-parabolic method that achieves second order accuracy through spatial interpolation. These second order methods and more are better at treating shocks in the flow resulting in monotonicity preserving solutions than first order schemes, although their shortcomings appear in complicated smooth solution structures [104] which can be handled better by schemes of higher order. In the next sections, we present two of these modern methods that are based on Godunov's method employing reconstruction techniques in treating discontinuities with no oscillations, these methods are referred to as *essentially non-oscillatory* (ENO) and *weighted essentially non-oscillatory* (WENO) methods.

4.3.1 Finite-Difference WENO Schemes

The Weighted ENO schemes [111, 112, 114, 115] and are based on the ENO schemes we have reviewed in the appendix (C). The ENO schemes have a criterion of choosing the stencil to represent the fluxes in the grid where the interpolation polynomial is the most smooth. In the WENO schemes we instead choose a convex combination of all of the stencil by assigning each stencil a proper weight. The essentially non-oscillatory property is still maintained through non-vanishing weights on the smooth stencils, and on the discontinuous stencils the weights are vanishing such that there is no contribution from the convex combination.

Suppose we have k stencils which we denote

$$S_j^{(\ell)} = (x_{j-\ell}, ..., x_{j-\ell+k-1}), \qquad \ell = 0, ...k-1. \tag{4.40}$$

Suppose further that associated with these stencils, are the following k interpolation polynomials to the numerical fluxes

$$p^{(\ell)}(x_{j+\frac{1}{2}}) \approx \hat{F}_{j+\frac{1}{2}}^{(\ell)}. \tag{4.41}$$

Then according to the WENO reconstruction, we choose the convex combination of these polynomials to interpolate the numerical fluxes at the cell boundaries of $\hat{F}(x_{j+\frac{1}{2}})$ such that

$$\hat{F}_{j+\frac{1}{2}} = \sum_{\ell=0}^{k-1} \omega_\ell p^{(\ell)}(x_{j+\frac{1}{2}}). \tag{4.42}$$

Where the weights ω_ℓ satisfy [114]

$$\sum_{\ell=0}^{k-1} \omega_\ell = 1, \quad and \quad \omega_\ell \geq 0, \tag{4.43}$$

and in the smooth regions coefficients ω_ℓ are accurate up to order $k-1$. We expect them to vanish in the discontinuous regions for the corresponding stencil. Due to the ENO property in the smooth regions of (C.10) the WENO schemes are accurate up to order $2k-1$ such that

$$\hat{F}_{j+\frac{1}{2}} = \sum_{\ell=0}^{k-1} \omega_\ell p^{(\ell)}(x_{j+\frac{1}{2}}) + \mathcal{O}(\Delta x^{(2k-1)}). \tag{4.44}$$

The weights ω_ℓ chosen in [112] as to maintain the essentially non-oscillatory property and the order of accuracy of the convex combination in all of the stencils. They are defined such that

$$\omega_\ell = \frac{\alpha_\ell}{\sum_{r=0}^{k-1} \alpha_r}, \qquad \ell = 0, ...k-1, \tag{4.45}$$

where

$$\alpha_\ell = \frac{d_\ell}{(\epsilon + \beta_\ell)^2}. \tag{4.46}$$

Here $\epsilon > 0$ is a small number that is included to avoid the denominator being zero and a good choice is between 10^{-5} to 10^{-7} without having any effects on the solution [115]; The d_ℓ are called *optimal weights* that are chosen to increase the order accuracy in the smooth regions such that

$$\omega_\ell = d_\ell + \mathcal{O}(\Delta x^{k-1}), \qquad \ell = 0, ...k-1, \tag{4.47}$$

with

$$\sum_{\ell}^{k-1} d_\ell = 1.$$

Finally, the β_ℓ measures the smoothness of the fluxes in their respective stencils $S_j^{(\ell)}$, that is the larger this value is then the less smooth the flux is. In this thesis, we use a third order WENO scheme [116] that is characterized by the following optimal weights

$$d_0 = \frac{2}{3}, \tag{4.48}$$

$$d_1 = \frac{1}{3}. \tag{4.49}$$

$$\tag{4.50}$$

and the smoothness indicators

$$\beta_0 = (f(u_{i+1}) - f(u_i))^2, \tag{4.51}$$

$$\beta_1 = (f(u_i) - f(u_{i-1}))^2. \tag{4.52}$$

$$\tag{4.53}$$

Chapter 5

Neutron Stars in *f(R)* Gravity

Models that aim to explain the cosmic acceleration observed from type Ia Supernovae, has garnered so much interest in the past decades. Among the proposed models, modified gravity constitutes a bold approach, as it aims to modify the Einstein field equations. In this thesis we focus on the $f(R)$ class of modified gravity theories [10, 11]. In particular, we adopt the Starobinsky R-squared model [122], corresponding to $f(R) = R + \alpha R^2$. This model is conformally equivalent to Einstein's theory of gravity and an additional light scalar field. The extra scalar field in these models has been shown to induce instabilities in low curvatures in some of the $f(R)$ models [117, 118], and that has led to an intensive search of viable $f(R)$ models that are matter dominated in the early universe times and with extra corrections that explain late time acceleration [119–121].

The Starobinsky model is one of the most viable $f(R)$ models [124], and it is consistent with the physical observations [123] as compared to most scalar-field theories. The study of $f(R)$ models under neutron stars is divided into two approaches, the first being the perturbative method - where $f(R)$ is considered a small perturbation from general relativity *e.g* [125] - and the non-perturbative method - where the entire $f(R)$ function is explicitly considered in the modified Einstein-Hilbert action *e.g* [132] (and this thesis). At the moment we know about the mass and radii of neutron stars than anything else related to its behavior at extreme conditions. Hence the mass-radius ($\mathcal{M}$-$\mathcal{R}$) diagram obtained from solving the full TOV equations (5.43)-(5.48) with an equation of state (EoS), is the best tool used to compare these alternate theories against each other and find the most viable one. The measured mass of static and spherically symmetric neutron stars was constrained by Chandrasekhar with an upper limit of $1.44 M_\odot$ for an EoS of degenerate matter. Although with new developments in the field considering different systems such as binary neutron stars [129] or different methods used [128], much more heavier neutron stars have been discovered. These heavier stars may contain phenomena that extends over general relativity, and more particularly with the 2017 gravitational detection GW170817 of merger of a binary neutron star system [130], the current upper limit is set at $2.16^{+0.17}_{-0.15} M_\odot$ [131]. Keep in mind that the true mass of the neutron star still remains a mystery as these measurements do not take into account a plethora of EoS and the interior of the neutron star is still not entirely understood.

In this chapter, we generate the mass-radius relation for several realistic equation of states while also varying the free parameter α. In the low values of α stiff terms emerge in the system, the previous studies have handled this by using runge-kutta methods with adaptive step size, see

e.g [132]. As we have mentioned in section 4.2.2, this approach leads to function evaluations that are subsequently discarded in the hunt for the optimal step size. In this thesis, we use an IMEX scheme as we will see, to treat these stiff terms.

5.1 Modified Equations

Let us look at one of the solutions to the field equations by R.C. Tolman [26] where a spherically symmetrical perfect fluid with an equilibrium distribution of matter. Its metric has the form

$$ds^2 = -e^{2\nu}dt^2 + e^{2\lambda}dr^2 + r^2(d\theta^2 + \sin^2\theta d\phi^2), \tag{5.1}$$

where $\nu = \nu(r)$ and $\lambda = \lambda(r)$. Of course outside this star we have a spherically symmetric vacuum such that this metric reduces to the Swarzschild solution.

We want to define the Einstein field equations for this stellar model, we take the approach that uses the equations (2.17). As we have introduced our energy-momentum tensor on equation (2.16), we use this to describe the matter inside the stellar model. As we assumed perfect fluid so that shear stress is negligible and static in that we exclude all pulsating or exploding. Therefore that makes our 4-velocities in equation (2.16) timelike 4-vectors. In order to obtain the t element we normalise our 4-velocities

$$\begin{aligned} -1 &= \mathbf{U}\cdot\mathbf{U}, && (5.2)\\ &= g_{ab}U^aU^b, && (5.3)\\ &= g_{tt}U^tU^t, && (5.4)\\ &= -e^{2\nu}U^tU^t, && (5.5)\\ e^{-\nu} &= U^t, && (5.6) \end{aligned}$$

which then means our 4-velocity is $\mathbf{U}= e^{-\nu}(1,\mathbf{0})$. Now looking at equation (2.16) we can obtain the elements of the energy-momentum tensor, also as it is symmetric it makes things easier, from our looking at our metric also we find that

$$\begin{aligned} T^{tt} &= \rho e^{-2\nu}, && (5.7)\\ T^{rr} &= pe^{-2\lambda}, && (5.8)\\ T^{\theta\theta} &= pr^{-2}, && (5.9)\\ T^{\phi\phi} &= pr^{-2}sin^{-2}\theta, && (5.10) \end{aligned}$$

and all the other elements are zero.

We now have the matter description for the line element (5.1), we obtain the geometrical description by deriving the explicit components of the Einstein tensor. From the definition of the Christoffel symbols (2.3), we substitute the nonzero components for the metric and its inverse

to obtain the non-vanishing Christoffel symbols

$$\begin{aligned}
\Gamma^t_{tr} &= \nu', && (5.11)\\
\Gamma^r_{tt} &= e^{2(\nu-\lambda)}, && (5.12)\\
\Gamma^r_{rr} &= \lambda', && (5.13)\\
\Gamma^r_{\theta\theta} &= -re^{-2\lambda}, && (5.14)\\
\Gamma^r_{\phi\phi} &= -re^{-2\lambda}sin^2\theta, && (5.15)\\
\Gamma^\theta_{r\theta} &= \frac{1}{r}, && (5.16)\\
\Gamma^\theta_{\phi\phi} &= -sin\theta\cos\theta, && (5.17)\\
\Gamma^\phi_{r\phi} &= \frac{1}{r}, && (5.18)\\
\Gamma^\phi_{\theta\phi} &= \frac{cos\theta}{\sin\theta}. && (5.19)
\end{aligned}$$

We substitute these Christoffel symbols into the definition of the Riemann curvature to obtain the Ricci tensor, which is also a diagonal tensor whose non-vanishing components are given by

$$\begin{aligned}
R_{tt} &= e^{2(\nu-\lambda)}[\nu'' + (\nu')^2 - \nu'\lambda' + 2r^{-1}\nu'], && (5.20)\\
R_{rr} &= -[\nu'' + (\nu')^2 - \nu'\lambda' + 2r^{-1}\lambda'], && (5.21)\\
R_{\theta\theta} &= 1 - e^{-2\lambda}[1 + r(\nu' - \lambda')], && (5.22)\\
R_{\phi\phi} &= sin^2\theta[1 - e^{-2\lambda}[1 + r(\nu' - \lambda')]]. && (5.23)
\end{aligned}$$

Contracting the diagonally symmetric Ricci scalar with the star's metric gives us the Ricci scalar such that

$$R = 2[r^{-2} - e^{-2\lambda}(\nu'' + (\nu')^2 - \nu'\lambda' + 2r^{-1}\nu' - 2r^{-1}\lambda' + r^{-2})]. \quad (5.24)$$

We then obtain the equations' (2.17) components such that for the G_{tt} component we obtain

$$\begin{aligned}
8\pi T_{tt} &= r^{-2} - e^{-2\lambda}(2r^{-1}\lambda' + r^{-2}), && (5.25)\\
8\pi\rho e^{2\nu} &= r^{-2}\frac{d}{dr}r(1 - e^{-2\lambda}), && (5.26)
\end{aligned}$$

where we divided by the g_{tt} component of the metric. Following Cooney *et. al* in [125] and Stephani in [40] we can make the define the change of variable by introducing

$$2m(r) = r(1 - e^{-2\lambda}), \quad (5.27)$$

then we can rewrite our equation for the potential λ as

$$e^{2\lambda} = \left(1 - \frac{2m}{r}\right)^{-1}. \quad (5.28)$$

Therefore now from equation (5.26) the first field equation has the form

$$\frac{dm(r)}{dr} = 8\pi\rho r^2. \quad (5.29)$$

Our newly introduced variable can be recovered by the means integrating from the center of the stellar model to its surface, assuming that the initial conditions of the stellar model were smooth *i.e* $m(0) = 0$ hence

$$m(r) = \int_0^r 4\pi\rho^2 dr + m(0), \tag{5.30}$$

this is referred to as the mass-energy of the stellar model.

We follow a similar approach to derive the second field equation, starting from the G_{rr} component, which is

$$8\pi T_{rr} = -r^{-2} + e^{-2\lambda}(r^{-2} + 2r^{-1}\nu'), \tag{5.31}$$

$$8\pi p e^{2\lambda} = -r^{-2} + e^{-2\lambda}(r^{-2} + 2r^{-1}\nu'), \tag{5.32}$$

where we divide by the g_{rr} component of the metric. Substituting with equation (5.27) and solve for the gradient of ν gives us

$$\frac{d\nu}{dr} = \frac{m + 4\pi r^3 p}{r(r - 2m)}. \tag{5.33}$$

There are now two ODE for the metric potentials, to close this system we require a relation of the stellar matter following the energy-momentum tensor components. We make use of the conservation equation (2.15) to the obtain the pressure gradient required in the star to maintain equilibrium distribution. By projecting the conservation equations along the 4-velocity of the static stellar model, hence the pressure only depends on r and (2.15) reduces to

$$\frac{dp}{dr} = -(\rho + p)\frac{d\nu}{dr}, \tag{5.34}$$

then substituting (5.33) we get our Oppenheimer-Volkoff equation of hydrostatic equilibrium as

$$\frac{dp}{dr} = -\frac{(\rho + p)(m + 4\pi r^3 p)}{r(r - 2m)}. \tag{5.35}$$

We now have four unknown variables which are λ, ν, p, and ρ, all as functions of the radial coordinate. We have managed to reduce the field equations 2.17 to these three ODEs. The foundation from analysing spherically symmetric models was first calculated by R.C. Tolman in [26] and [27], then in shortly J.R. Oppenheimer and G.M. Volkoff further extended the equations [31] in form hence are called the $Tolman-Oppenheimer-Volkoff$ equations. What we have done so far is to derive these equations (5.29),(5.33) and (5.35) in an attempt to solve the Einstein Field equations (2.17). We need to integrate these equations to find the matter components (m, p and ρ) and the source potential ν. Our model is almost complete, what's left to solve the above equations are the boundary conditions and the equations of state $p = p(\rho)$ for our star.

The model so far seems to be dependent on the total energy density ρ, this determined through a relation between p and ρ. Although one thing we need to be sure of is the dependence of these two matter variables on thermodynamic laws (e.g temperature, entropy) that affect the matter inside the star. The pressure p and the energy obviously depends on how many fluid elements are in the star *i.e* number of baryons n. Also from thermodynamics they would depend

on the fluid element's temperature to determine how fast they might be interacting with each other, we consider entropy s using the relation from their temperature such that

$$p = p(n, s), \tag{5.36}$$
$$\rho = \rho(n, s). \tag{5.37}$$

During the formation of the neutron star, its temperature rises rapidly and reaches $10^{11}K$ magnitudes, although there are lot of neutrinos are emitted and they carry most of the energy away with them and this leaves the newly formed neutron star with much less thermal energy $T << 10^{11}K$ after a few seconds [32]. We can then exclude all the thermal contributions and set $s = 0$, then our thermodynamic variables take the form

$$p = p(n), \tag{5.38}$$
$$\rho = \rho(n). \tag{5.39}$$

We then need to determine the central density value ρ_c and given the EoS that relates pressure and the energy density, then we can solve this system within the following boundary conditions.

We have to numerically integrate the stars' field equations from the origin $r = 0$ *i.e* center of the star, up to the surface of the star $r = R$, where R is the radius of the star. Inside the star the TOV equations are valid and one can integrate from $r << 1$. Outside the star we know that the geometry is described by the Schwarzchild metric [28]

$$ds^2 = -\left(1 - \frac{2M}{r}\right)dt^2 + \left(1 - \frac{2M}{r}\right)^{-1} dr^2 + r^2 d\Omega^2, \tag{5.40}$$

where

$$d\Omega^2 = d\theta^2 + sin^2\theta d\phi^2.$$

Outside the star, $\rho = 0$ hence from equation (5.29) we can see that the mass is a constant value given by

$$m(r) = M, \qquad r \geq R. \tag{5.41}$$

Then our metric potential is a function of the radial coordinate only, given by

$$\lambda = -\frac{1}{2} ln\left(1 - \frac{2M}{r}\right). \tag{5.42}$$

At the surface of the star, the pressure vanishes $p(R) = 0$ and the mass is $m(R) = M$, from matching the conditions outside and inside the star. We now have a complete stellar model that can be solved from the centre of the spherically symmetric with equilibrium distribution outward to the surface where the pressure vanishes and this is a consequence of the hydrostatic equation. After initially determining the central energy density ρ_c and the EoS that satisfies $\rho \geq 0$ and $p \geq 0$. We have managed to reduce our model from the Einstein field equations to a one parameter system.

Now let us derive the field equations for the general $f(R)$ Lagrangian density in (2.20) under the framework of a static spherically symmetric star with the metric (5.1) and the energy-momentum tensor is that of a perfect fluid (5.7). We have used substitution and the conservation

equation $\nabla_a T^{ab} = 0$ to reduce the general field equations to the following differential equations for the two radial functions

$$\frac{d\nu}{dr} = 4\pi\zeta r e^{2\lambda}p + \frac{\zeta r(e^{2\lambda}-1)f'}{2r} + \frac{\zeta r(f - Rf')e^{2\lambda}}{4} - \zeta f''Q, \tag{5.43}$$

$$\frac{d\lambda}{dr} = \frac{4\pi r e^{2\lambda}}{3f'}(2\rho + 3p) + \frac{(1-e^{2\lambda})}{2r} + \frac{r(f + Rf')e^{2\lambda}}{12f'} - \frac{rf''}{2^{f'}}\frac{d\nu}{dr}Q, \tag{5.44}$$

where

$$\zeta = \left(f' + \frac{r}{2}f''Q\right)^{-1}$$

and the variable Q was introduce to reduce the order of the differential equation for the Ricci scalar as it is a dynamic variable in the $f(R)$ theories and its DE are

$$\frac{dR}{dr} = Q, \tag{5.45}$$

$$\frac{dQ}{dr} = \left(\frac{d\lambda}{dr} - \frac{d\nu}{dr} - \frac{2}{r}\right)Q - \frac{f'''}{f''}Q^2 + \frac{e^{2\lambda}(2f - Rf')}{3f''} - \frac{8\pi e^{2\lambda}(\rho - 3p)}{3f''}, \tag{5.46}$$

although the conservation of the energy-momentum tensor leads to the same form for differential equation for pressure as

$$\frac{dp}{dr} = -(\rho + p)\frac{d\nu}{dr}. \tag{5.47}$$

We make a change of variable following (5.27) and using equation (5.44) we get the change of the mass of our stellar model with respect to the radial coordinate

$$\frac{dm}{dr} = \frac{m}{r} + \frac{d\lambda}{dr}(r - 2m). \tag{5.48}$$

Substituting the Starobinsky function into the TOV equations (5.43)-(5.45), we obtain the stars field equation in the R-squared model as

$$\frac{d\nu}{dr} = 4\pi\zeta r e^{2\lambda}p + \frac{\zeta(e^{2\lambda}-1)(1 + 2\alpha R)}{2r} - \frac{\zeta r\alpha r^2 e^{2\lambda}}{2 - 2\zeta\alpha Q}, \tag{5.49}$$

$$\frac{d\lambda}{dr} = \frac{4\pi r e^{2\lambda}(2\rho + 3p)}{3(1 + 2\alpha R)} + \frac{(1-e^{2\lambda})}{2r} + \frac{e^{2\lambda}(2R + 3\alpha R^2)}{12(1 + 2\alpha R)} - \frac{r}{(1 + 2\alpha R)}\frac{d\nu}{dr}Q, \tag{5.50}$$

$$\frac{dR}{dr} = Q, \tag{5.51}$$

$$\frac{dQ}{dr} = \left(\frac{d\lambda}{dr} - \frac{d\nu}{dr} - \frac{2}{r}\right)Q - \frac{Re^{2\lambda}}{6\alpha} - \frac{8\pi e^{2\lambda}(\rho - 3p)}{6\alpha}, \tag{5.52}$$

where

$$\zeta = \frac{1}{(1 + \alpha(2R + rQ)}. \tag{5.53}$$

As we consider the neutron star's matter source to be a perfect fluid, its hydrostatic equilibrium (5.47) is still the same in the R-squared model

$$\frac{dp}{dr} = -(\rho + p)\frac{d\nu}{dr}. \tag{5.54}$$

The mass of the neutron star is recovered through the integration of

$$\frac{dm}{dr} = \frac{m}{r} + \frac{d\lambda}{dr}(r - 2m). \tag{5.55}$$

Such that $m(r)$ is the effective mass and if the radius of the neutron star is r_s the total effective mass of the neutron star observed outside the star is denoted $m(r_s) = M$. The field equations of modified gravity allows for the existence of stars with high mass to radius ratios [134]. This result can be demonstrated analytically under certain simplifying assumptions. For example, in GR, assuming the interior of the star is made up of a constant density, incompressible fluid, one can show that the mass to radius ratio is bounded by

$$\frac{2M}{R} \leq \frac{8}{9}. \tag{5.56}$$

This is known as the Buchdal-Bondi limit. However, in f(R) it was shown that this can be higher [135].

In the R-squared model when $\alpha \to 0$, the modified Einstein-Hilbert action reduces to standard general relativity form. This effect is inherent to the $f(R)$ system of equations, particularly the modified TOV equations (5.49)-(5.55), such that in the limit $\alpha \to 0$ solving these equations' solution is closer to the standard general relativity instead. This limit introduces stiffness into the last two terms of equation (5.52), which will require to be solved by an Implicit-Explicit scheme. Before discussing the numerical method we have used, we need to touch on the boundary conditions. The equations are integrated from the center of the star by imposing the initial conditions

$$\rho(0) = \rho_c, \tag{5.57}$$
$$m(0) = 0, \tag{5.58}$$
$$Q = 0. \tag{5.59}$$

Since ν appears only differentially in the TOV equations, it can always be rescaled by a constant term. We therefore pick the initial condition $\nu(0) = 1$. The only quantity left is the Ricci scalar. We use a shooting method to pick initial conditions for R such that $R = 0$ at infinity. Consequently, the boundary value problem was reduced to an initial value problem, such that a shooting method is employed to find a root to the function

$$Y(R_0) = X(R_0, r_{radius}) - R_{bc},$$

where $X(R_0, r_{radius})$, and R_{bc} are the values of the Ricci scalar at the boundary as a function of the initial condition. The root-finding methods discussed in appendix (A) were used to find the roots of this function once an initial guess has been provided. Some of these methods are not defined for certain values of R_0 or require the knowledge of dX/dR_0, which leads to ill-behaved solutions with very slow or no convergence at the boundary. In this thesis the Ridder's method, which requires an interval containing the right initial guess R_0, performed with much better convergence to the boundary condition compared to the other methods.

The numerical method we used was based on an IMEX scheme code that was incorporated in a root-finding method, for the initial values of the Ricci scalar. The IMEX scheme integrated the field equations, from a small value of r close to zero, to avoid $1/r$ terms which become

singular at $r = 0$. The radius of the star was taken as the last value of the radial coordinate, *i.e* where the pressure vanishes. Unlike previous studies, e.g [136] where the integration is stopped at the surface of the star, we continue the integration of ν, λ, R, and Q equations in vacuum up to some large radius. With this approach, the solution in the exterior region of the neutron star is not restricted to that of Schwarzschild. This is consistent with the fact that Birkhoff's theorem does not generally hold in modified theories of gravity [137]. If one was interested in solutions that obey Birkhoff's theorem, then it would be necessary impose the junction conditions [138]

$$[R] = 0, \qquad [\nabla_\lambda R] = 0, \tag{5.60}$$

where [ ] denotes the discontinuity at the edge of the star. However, following [132], we do not do that in this thesis.

5.2 Results and Discussion

We produce the $\mathcal{M} - \mathcal{R}$ relation by solving the modified field equations (5.49)-(5.55) along with the boundary conditions, and an EoS describing the behavior of the nuclear matter of the neutron star. Since the behavior is still not well understood in the field, there has been numerous equations of state that have been proposed and they lead to different mass-radius relations. In this thesis we considered seven realistic equations of states, which are given in the Table 5.1,

Table 5.1: The EoS we used, which came in the form of tabulated values of density and pressure. The EoS data files were obtained from the publicly available Lorene code [139]

EoS	Ref.	EoS	Ref.
SLy4	[140]	BALBN1H1	[143]
FPS	[141]	BBB2	[144]
AKMAL	[142]	BPAL12	[145]

We do not use analytic representations of these EoS but rather we use them in tabulated form employing linear interpolation on a logarithmic scale. We generated the mass-radius equations for different values of α between 0 and 100, to show the effects of the parameter on the structure of the star.

Referring to figure (5.1), we note that for models with $\alpha \leq 1$, the masses are very close to the general relativity model. The maximum mass for GR was recorded as $2.04 M_\odot$, which is less than the mass limit. The maximum mass for the models with $\alpha \leq 1$ also satisfies this limit. Although when increasing the value of α, we note that the corresponding masses get to be larger than the GR model. As seen in the left panel, the model $\alpha = 100$ records the smallest radius range of the neutron star such that the star reaches its maximum mass at a smaller radius compared to the other models. In the right panel, the model $\alpha = 20$ reaches higher masses faster than the other models with an almost significant maximum mass point. Additionally, the $\alpha = 100$ model appears to be moving faster than all the models with respect to the central density up to the point of maximum mass. As the star continues to increase in its central density, the change in its mass almost remains constant and above the GR model.

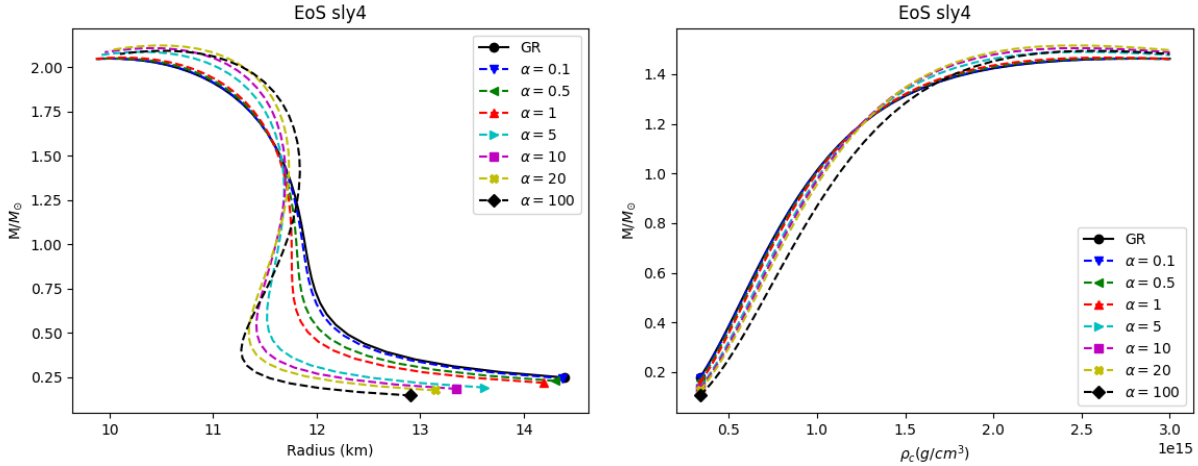

Figure 5.1: *Left panel:* The gravitational mass of the star as a function of its radius obtained from the Sly4 equation of state. Different values of α in $f(R) = \alpha R^2 + R$ are represented in dashed different colored lines, and the general relativity in the solid black line. The maximum and minimum mass are marked with the respective markers as shown in the legend for different α values. *Right panel:* The gravitational mass as a function of the central density for different values of α.

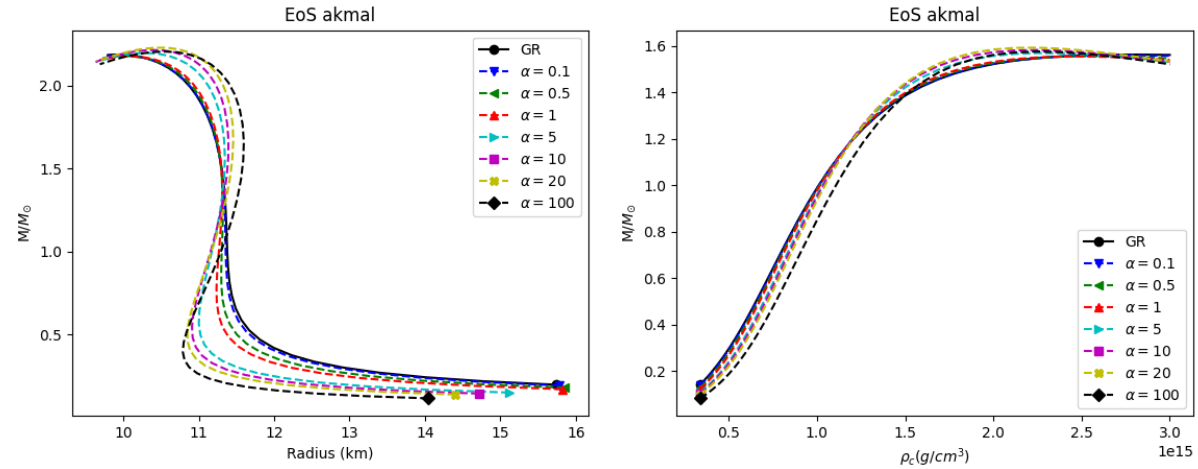

Figure 5.2: *Left panel:* The gravitational mass of the star as a function of its radius obtained from the AKMAL equation of state. Different values of α in $f(R) = \alpha R^2 + R$ are represented in dashed different colored lines, and the general relativity in the solid black line. The maximum and minimum mass are marked with the respective markers as shown in the legend for different α values. *Right panel:* The gravitational mass as a function of the central density for different values of α.

The AKMAL equation of state in left panel of figure (5.2) shows a maximum mass of about $2.18 M_\odot$ for the GR model. The masses of models of $\alpha \geq 5$ appears to be decreasing faster past the maximum point with respect to the radius. This can also be seen in the right panel where the mass of the star seems to steadily increase with respect to the central density up to the point of maximum mass, then the masses of these models decrease further than the GR and

$\alpha \leq 1$ models for equilibrium. The model $\alpha = 20$ achieve the largest maximum mass of about $2.22M_{\odot}$ which is above the limit of [131].

In the figures (5.3) and (5.4) we see that the maximum masses for the FPS and BBB2 equations of state are about $1.96M_{\odot}$ and $1.91M_{\odot}$ respectively. The models with $\alpha \geq 1$ for both EoS agree with the GR model for small radii. The BBB2 model appears to record the smallest radii for the models $\alpha = 1$ and $\alpha = 20$ as compared to the other models considered. Both the FPS and BBB2 EoS realize the largest maximum mass with the model $\alpha = 20$ for values $1.48M_{\odot}$ and $1.99M_{\odot}$ respectively.

The left panel of the figure (5.6) shows the masses of the star for different models, decreasing slowly and followed an abrupt decrease past the 12.7km radius. The right panel exhibits the sharp increase of the masses in the lower central densities, followed by a steady increase up to the point of maximum mass. The model $\alpha = 100$, realizes central density values are very large with small masses compared the GR model in the higher central densities region. The maximum mass for the GR model is $1.61M_{\odot}$, which is below the recorded limit.

The maximum mass obtained from the Sly4 and AKMAL EoS are consistent with the mass limit given in ([131]) within GR. Regardless of the EoS, the maximum mass seems to increase with the increase of α in the case of $\alpha \geq 20$. Then after it reaches a maximum, it slightly decreases when $\alpha > 20$. This result is different from the results given in [132], where for small values of α they recorded a maximum mass decrease down to a low point, followed by a slight increase for large values of α.

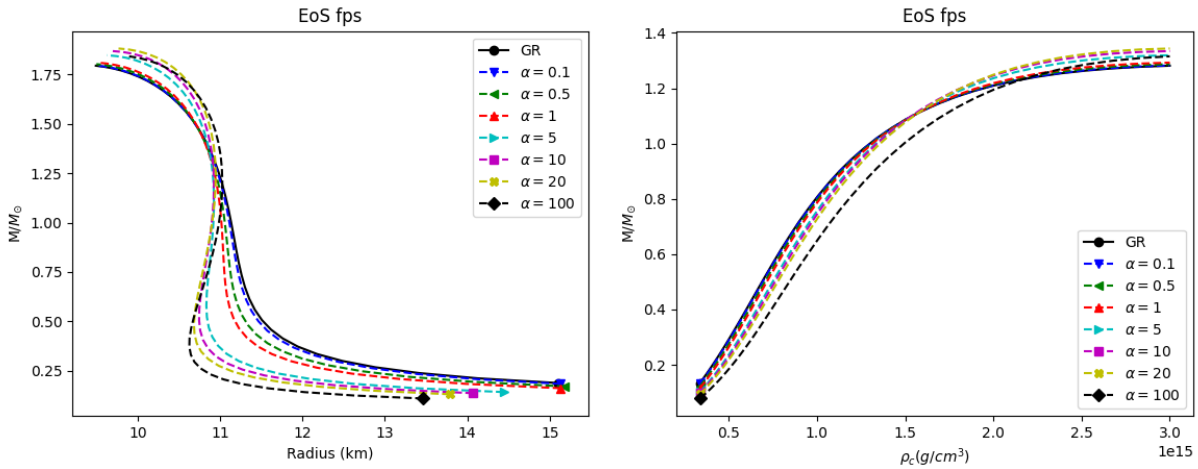

Figure 5.3: *Left panel:* The gravitational mass of the star as a function of its radius obtained from the FPS equation of state. Different values of α in $f(R) = \alpha R^2 + R$ are represented in dashed different colored lines, and the general relativity in the solid black line. The maximum and minimum mass are marked with the respective markers as shown in the legend for different α values. *Right panel:* The gravitational mass as a function of the central density for different values of α.

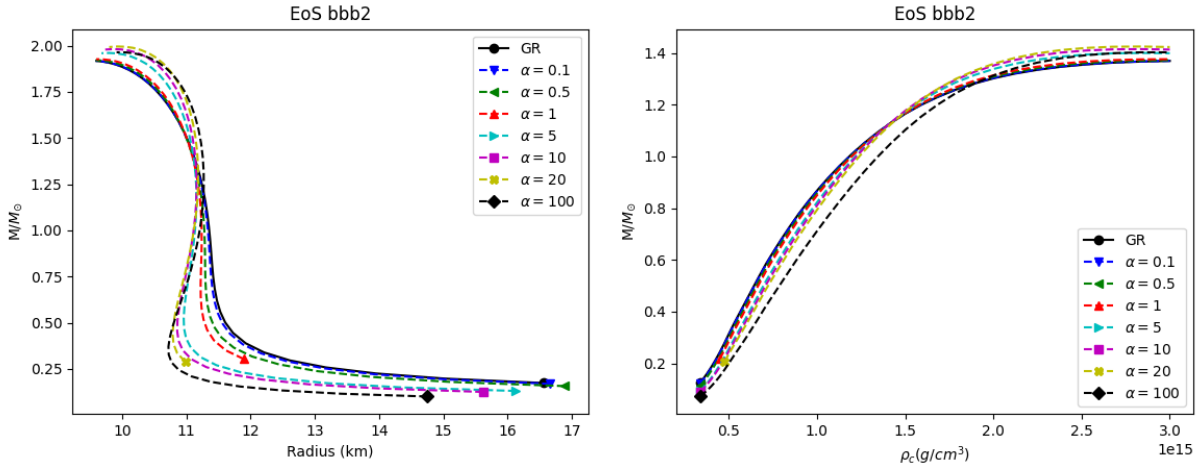

Figure 5.4: *Left panel:* The gravitational mass of the star as a function of its radius obtained from the BBB2 equation of state. Different values of α in $f(R) = \alpha R^2 + R$ are represented in dashed different colored lines, and the general relativity in the solid black line. The maximum and minimum mass are marked with the respective markers as shown in the legend for different α values. *Right panel:* The gravitational mass as a function of the central density for different values of α.

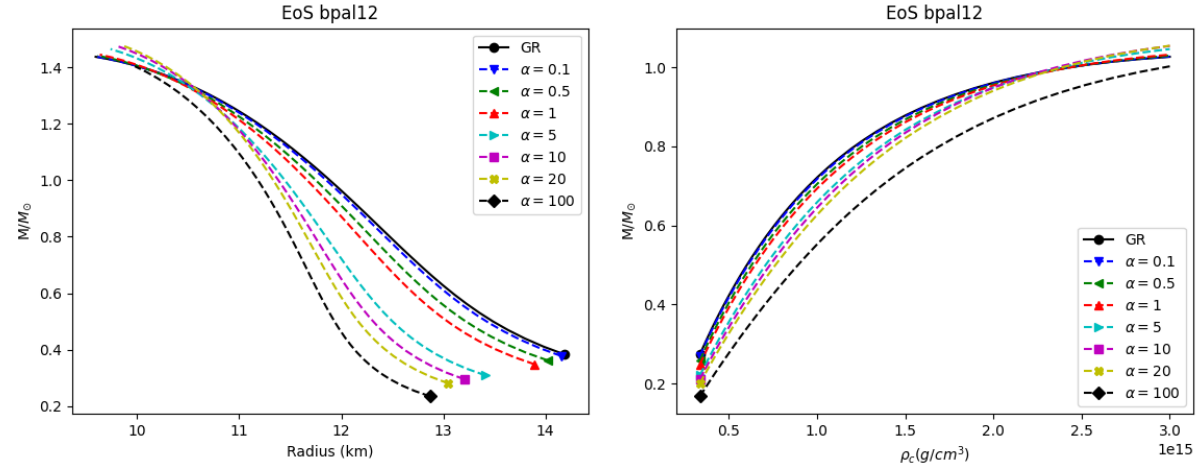

Figure 5.5: *Left panel:* The gravitational mass of the star as a function of its radius obtained from the BPAL12 equation of state. Different values of α in $f(R) = \alpha R^2 + R$ are represented in dashed different colored lines, and the general relativity in the solid black line. The maximum and minimum mass are marked with the respective markers as shown in the legend for different α values. *Right panel:* The gravitational mass as a function of the central density for different values of α.

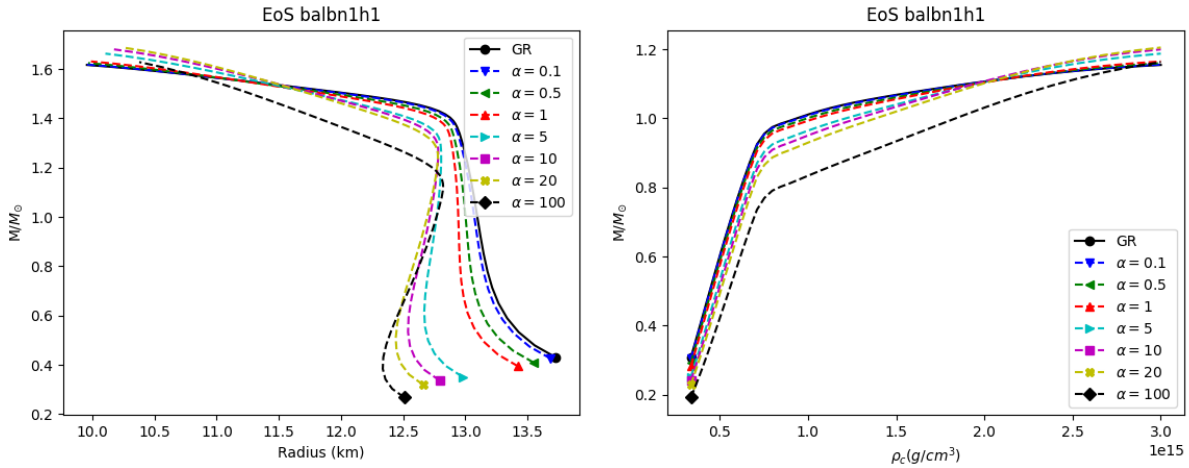

Figure 5.6: *Left panel:* The gravitational mass of the star as a function of its radius obtained from the BALBN1H1 equation of state. Different values of α in $f(R) = \alpha R^2 + R$ are represented in dashed different colored lines, and the general relativity in the solid black line. The maximum and minimum mass are marked with the respective markers as shown in the legend for different α values. *Right panel:* The gravitational mass as a function of the central density for different values of α.

Chapter 6

Radial Oscillations

Neutron stars are one of the representations of final state for highly dense relativistic stars. As we do not know much about the matter configurations inside the star, their radial oscillations allows us to learn more about their internal structure. The radial oscillations of non-rotating symmetric relativistic stars were investigated by Chandrasekhar [146] by studying linear perturbations from a hydrostatic equilibrium configuration governed by the Tolman-Oppenheimer-Volkov solutions (5.1). The main equations can be cast as an eigenvalue problem to obtain a complete and discrete set of frequencies for the oscillations. The turning point of the star's stability is characterized as the point where the gravitational mass as a function of the central energy density $M(\rho_c)$ has reached its maximum. Increasing the central energy density more than the critical energy density results in the star collapsing *i.e moving from stability into an unstable configuration*. This characterizes the point of emergence of a zero-frequency oscillation [147].

Since Chandrasekhar's work, the radial oscillations have been extensively investigated for different equations of states [147–149,151] (and references therein). The results are complemented in [154] by presenting the radial oscillations with lowest frequencies for various equations of state. Radial oscillations have since been attributed to significant events like the shuttering of a neutron star's crust [155], the merging of a highly eccentric binary neutron star system [156]. With all the recent developments, the stability of a non-rotating star can be analyzed by obtaining its fundamental frequencies, such that purely imaginary frequencies signal instability in the radial oscillation. Furthermore, this knowledge form the base to be extended to the radial oscillations of uniformly rotating stars [157].

Several methods have been used to compute the radial oscillation modes, see eg. [150] for a comprehensive review. In this thesis, we employ two methods based on linear perturbation theory. The first method is based on perturbing the ADM equations leading to a coupled system of PDEs and the other method is based on perturbing the TOV equations, leading to an eigenvalue problem that we solve via the shooting method. As we shall see, the linearized ADM equations contain terms that get stiffer as we approach the surface of the stellar model. Previous studies e.g. [148, 149] have dealt with this by using the Hamiltonian constraint to eliminate the stiff terms. We do not follow this route here because i) we aim to demonstrate the feasibility of the IMEX scheme to deal with stiffness in PDEs, and ii) using the linearized Hamiltonian constraint is impractical (due to the number of terms involved) in theories beyond GR. We compare the results from the IMEX scheme with those obtained by solving the eigenvalue problem via the

shooting method.

6.1 The Perturbation Equations

We consider small perturbation around the star's model, such that the metric of the new system is

$$\bar{g}_{ab} = g_{ab} + \hat{h}_{ab}, \tag{6.1}$$

where $\hat{h}_{ab} = \delta g_{ab}$ is the time-dependent perturbation metric and all perturbed variables are denoted with a hat, and g_{ab} is our background metric (5.1). The lapse function in the background spacetime is given by

$$\alpha = \sqrt{-g_{00}} = e^{\nu}. \tag{6.2}$$

We assume a vanishing shift vector in the background metric, which gives us the normal vector of the spacetime as

$$n^a = (e^{-v}, \mathbf{0}). \tag{6.3}$$

The last ADM variable, the spatial extrinsic curvature can be obtained through the equation (3.81). Note that the background spatial metric is independent of time, the spatial extrinsic curvature then takes the form

$$K_{ij} = 0. \tag{6.4}$$

In chapter 3 we have derived the evolution and constraint equations for the background metric, we now derive the perturbation evolution and constraint equations. By perturbing the energy-momentum tensor, guarantees the perturbation of the of the star's matter where the pressure perturbation is given by

$$\hat{p} = \frac{dp}{d\rho}\hat{\rho} = C_s^2\hat{\rho}, \tag{6.5}$$

where C_s is the sound speed.

The ADM system (3.67)-(3.66) is then perturbed by substituting the perturbed variables such that for example

$$\begin{aligned} K_{ij} &\rightarrow K_{ij} + \delta K_{ij} && (6.6)\\ &= K_{ij} + \hat{K}_{ij}. && (6.7) \end{aligned}$$

We consider the terms higher than second order negligible, and the perturbation evolution equations after some manipulations take the form

$$\begin{aligned} \partial_t\hat{h}_{ij} &= \hat{\beta}^k\partial_k\gamma_{ij} + \gamma_{ki}\partial_i\hat{\beta}^k + \gamma_{jk}\partial_j\hat{\beta}^k - 2e^{\nu}\hat{K}_{ij}, && (6.8)\\ \partial_t\hat{K}_{ij} &= -\partial_i\partial_j\alpha + \Gamma^k_{ij}\partial_k\hat{\alpha} + \hat{\Gamma}^k_{ij}\partial_k e^{\nu} + \alpha\big(R_{ij} + 4\pi\gamma_{ij}(p-\rho)\big) && (6.9)\\ &+ e^{\nu}\big[\hat{R}_{ij} + 4\pi\big(\gamma_{ij}(p-\rho) + \hat{\rho}(C_s^2 - 1)\big)\big]. \end{aligned}$$

Similarly, the constraint equations (3.50) and (3.51) are substituted by the perturbed variables. Then up to first order perturbations the momentum and Hamiltonian constraint equations take the form

$$\begin{aligned} \gamma^{jk}(\partial_i\hat{K}_{jk} - \partial_j\hat{K}_{ki} - \Gamma^n_{ik}\hat{K}_{jn} + \Gamma^n_{kj}\hat{K}_{ni}) &= -8\pi(p+\rho)\hat{u}_i, && (6.10)\\ \gamma^{ij}\hat{R}_{ij} - \hat{h}^{ij}R_{ij} &= 16\pi\hat{\rho}, && (6.11) \end{aligned}$$

where $\hat{h}^{ij} = \bar{g}^{ij} - \gamma^{ij}$. The perturbed system (6.8) - (6.11) form a spherically symmetric system inherited from the background system. Therefore, the oscillations are carried only in the radial coordinate (t, r). Spherical tensor harmonics Y^a_{lm} allow us to decouple the coordinates in the system. Which can be used to expand the perturbed metric h_{ab} and extrinsic curvature K_{ij} along with the matter variables ρ, u_i as it was done in [148]. Such that the radial oscillations are encoded in $l = 0$ with no angular dependence, nor any gravitational radiation beyond the surface of the stellar model. From here we drop the hats in the perturbation equations for readability.

6.2 The Radial Equations

The system needs to be simplified by means of setting gauge conditions for the lapse function α and shift vector β^k, we then set

$$\alpha = e^{\nu} S_1(t, r), \tag{6.12}$$
$$\beta_k = r e^{2\lambda} S_2(t, r), \tag{6.13}$$

for arbitrary spherical harmonics coefficients in the (t, r) plane. Along with the spatial metric's and extrinsic curvature's expansions as

$$h_{ij} = \begin{pmatrix} r e^{2\lambda} S_3(t, r) & 0 & 0 \\ 0 & r^2 T(t, r) & 0 \\ 0 & 0 & r^2 sin^2\theta T(t, r) \end{pmatrix}, \tag{6.14}$$

$$K_{ij} = -e^{-\nu} \begin{pmatrix} e^{2\lambda} K_1(t, r) & 0 & 0 \\ 0 & \frac{1}{2} r^2 K_2(t, r) & 0 \\ 0 & 0 & \frac{1}{2} r^2 sin^2\theta K_2(t, r) \end{pmatrix}. \tag{6.15}$$

We now consider a few constraints about the spherical harmonics coefficients chosen before substituting them. Using the gauge freedom in the shift vector, we consider a vanishing shift and set $S_2(t, r) = 0$. Also set an initial condition on the angular components of the spatial matrix such that $T(t, r) = 0$ at $t = 0$. Additionally, the momentum constraint (6.10) reduces to a simple value of $K_1(t, r)$ when we consider a vanishing extrinsic curvature's variable $K_2(t, r)$, such that inside the stellar model we have

$$K_1(t, r) = 4\pi r e^{2\nu}(p + \rho)u = e^{2\nu - 2\lambda}(\lambda' + \nu')u, \tag{6.16}$$

where in the second equality we used $4\pi r e^{2\lambda} = \lambda' + \nu'$. Lastly, expansion for the energy density perturbation variable is chosen to further simplify the resulting equations, set as

$$H(t, r) = \frac{C_s^2}{p + \rho} \rho(t, r), \tag{6.17}$$

along with the velocity's expansion

$$u = -e^{\nu} u(t, r). \tag{6.18}$$

We substitute the expansions and implement the gauges $S_2 = T = K_2 = 0$ to find that the non-vanishing components of the Ricci scalar perturbations take the form

$$R_{rr} = S_3(4\lambda' + \frac{1}{r}) + S_3', \tag{6.19}$$

$$R_{\theta\theta} = 3S_3(\frac{r}{2} - r^2\lambda')e^{-2\lambda} + \frac{3}{2}r^2 S_3' e^{-2\lambda}, \tag{6.20}$$

$$R_{\phi\phi} = \frac{1}{2}S_3(r - \lambda' r^2 + e^{-2\lambda})e^{-2\lambda}sin^2\theta + \frac{1}{2}S_3' r^2 e^{-2\lambda}sin^2\theta. \tag{6.21}$$

The expansions are then substituted into the evolution equations, which results in a simpler set of evolution equations for the perturbations

$$\partial_t H = e^{2\nu-2\lambda}\big[C_s^2\partial_r u + u\big(C_s^2(\frac{2}{r} - 2\lambda') + \nu'(C_s^2 - 1)\big)\big], \tag{6.22}$$

$$\partial_t u = \partial_r H + H(\nu' + \lambda') + S_3(r\nu' + \frac{1}{2}), \tag{6.23}$$

$$\partial_t S_3 = 8\pi(p + \rho)e^{2\nu}u. \tag{6.24}$$

The Hamiltonian constraint equation (6.11) reduces to the form

$$8\pi e^{2\lambda}H(t,r)\frac{p+\rho}{C_s^2} = \partial_r S_3 + 2(r^{-1} - \lambda')S_3. \tag{6.25}$$

Using the momentum constraint equation (6.16), we can rewrite the evolution equations in a conservative form such that

$$\partial_t H + \partial_r(C_s^2 e^{2\nu-2\lambda}u) = e^{2\nu-2\lambda}[C_s^2(\frac{2}{r} - \nu') - \nu' + 2C_s C_s']u, \tag{6.26}$$

$$\partial_t u - \partial_r(H + \frac{r}{2}S_3) = -r(\lambda' - \nu')S_3 + S_3 - 4\pi r e^{2\lambda}(\rho + p)(1 - C_s^2)\frac{H}{C_s^2}, \tag{6.27}$$

$$\partial_t S_3 = 8\pi(\rho + p)e^{2\nu}u. \tag{6.28}$$

To solve the conservative system of differential equations, we integrate from the center of the stellar model to its surface. We therefore require initial and boundary conditions for the variables H, u and S_3. We require the quantities to be regular at $r = 0$. Due to the symmetry of the problem, we achieve this by imposing mirror symmetric boundary conditions at the center. At the surface of the star $r = R$, the Lagrangian pressure perturbation is required to vanish. This is the perturbation that is measured by an observer comoving with the star's fluid such that when they are at r in the background spacetime, then they are at $r + \xi(t, r)$ in the perturbed spacetime. The function $\xi(t, r)$ measures radial displacements of the star's fluid elements such that the Lagrangian pressure is

$$\Delta p(t, r) \approx \hat{p} + p_0'\xi, \tag{6.29}$$

where $\hat{p}$ is Eulerian pressure perturbation (6.5) and p_0 is the pressure at origin. Therefore, the observer's change in radial displacement along their world line with respect to t, is equivalent to the radial perturbation component of the fluid's 4-velocity such that

$$\partial_t \xi = e^{\nu-2\lambda}\hat{u}_r. \tag{6.30}$$

The conservation of matter along the radial displacement with respect to the 4-velocity of the fluid, combined with the definition of adiabaticity of the fluid gives us the Lagrangian pressure perturbation such that

$$\Delta p = -\Gamma_1 p r^{-2} e^{-\nu} (r^2 e^{-\nu} \xi)'. \tag{6.31}$$

Introducing a renormalization variable such that

$$\zeta = r^2 e^{-\nu} \xi, \tag{6.32}$$

translates the vanishing of the Lagrangian pressure perturbation at the surface to the condition

$$\zeta'|_{r=R} = 0. \tag{6.33}$$

As the condition for $\Gamma_1 p = 0$ is only true for certain stellar bodies where this product is not finite and nonzero at the surface [150], which we don't consider in this thesis. Now combining (6.30) and (6.18), the boundary condition (6.33) transforms to a condition for the 4-velocity at the surface such that

$$u'(R) = 2u(R)\left(\lambda'(R) - \frac{1}{2}\nu'(R) - \frac{1}{R}\right). \tag{6.34}$$

The value of the 4-velocity obtained from the above differential equation at the surface is used to obtain the other two variables H and S_3. Towards the surface of the star we have that $C_s^2 \to 0$, which makes (6.26) an ordinary differential equation for H, and the last term of (6.27) becomes stiffer with the decreasing sound speed. The Einstein field equations derived with the renormalized displacement function ζ, reduces the system to a wave equation given by

$$W \frac{\partial^2 \zeta}{\partial t^2} = \frac{\partial}{\partial r}\left(P \frac{\partial \zeta}{\partial r}\right) + Q\zeta, \tag{6.35}$$

where

$$W = (p+\rho) r^{-2} e^{2\lambda+\nu}, \tag{6.36}$$

$$P = (p+\rho) r^{-2} C_s^2 e^{\lambda+3\nu}, \tag{6.37}$$

$$Q = (p+\rho) r^{-2} e^{\lambda+3\nu}\left((\nu')^2 + 4 + \frac{\nu'}{r} - 8\pi^{2\lambda} p\right). \tag{6.38}$$

To obtain physical solutions for the renormalized displacement function, the wave equation is integrated after an initial displacement is specified along with the boundary conditions

$$\zeta(t, r = R)' = 0. \tag{6.39}$$

The fluid is assumed to be at rest at origin, and from the boundary condition (6.33) follows (6.39).

6.3 Eigenvalue Problem

Suppose we assume that the displacement of the star's fluid has a sinusoidal time dependence such that

$$\zeta(t, r) = \chi(r) e^{i\omega t}. \tag{6.40}$$

Substituting this form of displacement in (6.35), reduces the wave equation to a linear ordinary differential equation for $\chi(r)$. Which is an eigenvalue problem with ω as the angular frequency and $\chi(r)$ as the amplitude,

$$\frac{d}{dr}\left(P\frac{d\chi}{dr}\right) + (Q + \omega^2 W)\chi = 0. \tag{6.41}$$

Following the boundary conditions for the amplitude to close off the system as

$$\chi(t, r = R)' \;=\; 0. \tag{6.42}$$

The system (6.41) along with the boundary condition (6.42), form a Sturm-Liouville problem which uniquely solves for the eigenvalues $\omega^2 \in \mathbb{R}$ and their corresponding eigenfunctions $\chi(r)$. Although there are two cases here for the present harmonics based on the value of the frequency viz.

- $\omega^2 \geq 0 \implies \omega \in \mathbb{R}$,
- $\omega^2 < 0 \implies \omega \in \mathbb{I}_m$,

which corresponds to pure oscillatory modes, and damped or exponentially growing solutions respectively. Negative values of the frequency ω indicate instabilities in the radial oscillations before the Schwarzschild limit is met. In the stellar model we are dealing with, the mass of the star as a function of the central density reaches a point of maximum such that $dM/d\rho_c = 0$. For the fundamental mode, unstable radial oscillations correspond to central densities larger than the critical density ρ_{crit} at the maximum mass, which is $dM/d\rho_c < 0$. Hence, the maximal point of the mass marks the limit of stable radial oscillations, such that the star has to transition into a state of gravitational collapse to maintain a larger density.

In this thesis, we are interested in obtaining the frequencies of a star whose matter is governed by a polytropic equation of state. To obtain the frequencies, we integrate the system (6.26) - (6.28) by discretizing it with finite differencing. Then implement a third order WENO method along with an IMEX to handle the stiff terms in the differential equation of the velocity. We were able to recover the frequencies of the system by applying a Fourier transformation to the numerical solutions obtained from the IMEX-WENO method.

To verify the IMEX-WENO frequencies obtained, we implement an alternate method by solving the Sturm-Liouville equation (6.41). We first reduce its order by introducing an extra variable such that

$$\frac{d\chi}{dr} \;=\; \frac{\eta}{P}, \tag{6.43}$$

$$\frac{d\eta}{dr} \;=\; -(\omega^2 W + Q)\chi. \tag{6.44}$$

The boundary conditions at the origin are obtained through Taylor expansion of the variable $\chi(r), \eta(r)$ around the origin, and $\chi(r) \approx \chi_0 r^3 + \mathcal{O}(r^3)$ and $\eta(r) \approx \eta_0 + \mathcal{O}(r^2)$. Therefore, the initial values are related through $\chi_0 = \eta_0/3P_0$. At the surface of the star, we implement a shooting method by finding the frequency ω that corresponds to the root of the function $Y(\omega) = \chi(R, \omega)' - \chi'_{bc}$.

6.4 Results and Discussion

We use a polytropic EoS of the form

$$p = K\rho^{\Gamma}, \tag{6.45}$$

where where $K = 100$ is the adiabatic constant and $\Gamma = 2$ the adiabatic index. At $t = 0$ the initial value for the velocity perturbation u was set to a Gaussian pulse $u = Ae^{((r-\mu)^2/\sigma^2)}$, with the initial amplitude $A = 0.001$, $\mu = 0$, and $\sigma = 2$. The rest of the perturbation variables were set to 0 initially. We confirmed that the initial data satisfies the Hamiltonian constraint. The complete system is hyperbolic and in conservative form, which allowed us to discretize its space and time by the third order WENO scheme. The discretized system was evolved using the WENO method to obtain the numerical solution throughout time. This was then converted from the space and time domains, to their frequency domain using the Fast Fourier Transform (FFT) method. The Sturm-Liouville problem was also solved for its eigenvalues for verifying the IMEX-WENO scheme.

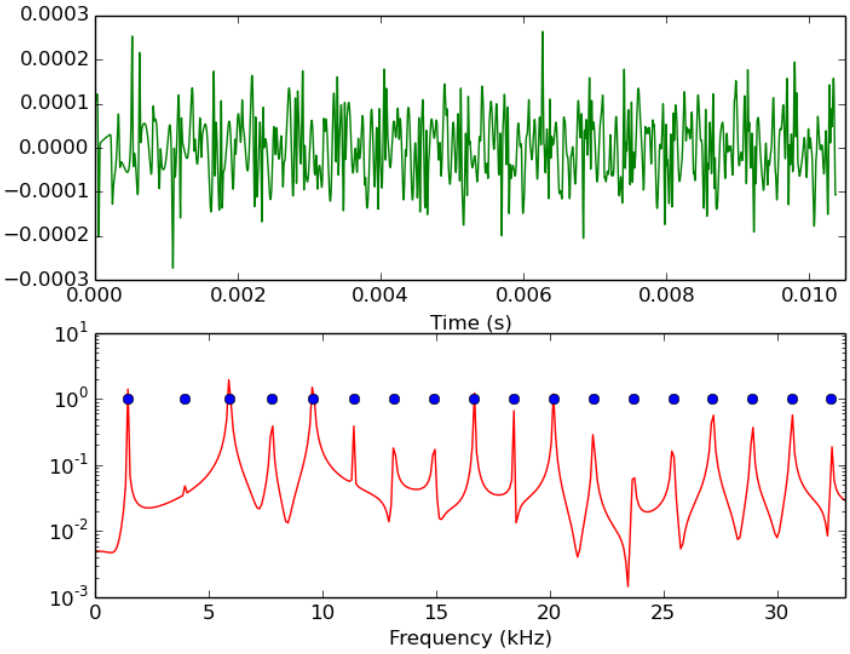

Figure 6.1: *Upper panel:* The spectrum mode of the numerical solution to the perturbation velocity in the time domain. Where ρ_c was set to 7.9056e14 g/cm^3, leading to a stable NS model with mass 1.4 solar mass and radius 14.15 km. *Lower panel:* The spectrum of the frequencies obtain from the FFT of the above solution and the frequencies obtained from the Sturm-Liouville problem are in circles.

The first eighteen frequencies are shown in lower panel of figure (6.1). The peaks in the frequency domain obtained from the FFT profiles coincide with the eigenfrequencies of the Sturm-Liouville problem, which are represented in circles. We compared the frequencies from the two methods up the 3rd decimal place in table (6.1).

Mode	Time domain (kHz)	Eigenfrequencies (kHz)	Relative Error (%)
F	1.443	1.447	0.30
H1	3.955	3.955	0.00
H2	5.916	5.885	0.50
H3	7.775	7.815	0.50
H4	9.589	9.551	0.40
H5	11.379	11.384	0.10
H6	13.154	13.121	0.30
H7	14.920	14.954	0.20
H8	16.678	16.691	0.10
H9	18.433	18.428	0.02
H10	20.183	20.164	0.10

Table 6.1: The first 11 frequencies obtained from FFT of the time domain and the eigenfrequencies are presented in the first and second column respectively. The third column has their respective errors.

The fundamental mode of this stellar model was found to be $\omega = 1.443kHz$. The fact that this value is not imaginary is indicative of the stability of this model to radial perturbations. This is consistent with other results in the literature, [158].

Chapter 7

Conclusion

In this thesis, we have studied two distinct problems described by systems of differential equations with stiff source terms. In Chapter 5, we studied the modified TOV equations for $f(R) = R + \alpha R^2$, with various realistic EoS. The resulting system of ODEs were found to contain stiff terms associated with the limit $\alpha \to 0$. In chapter 6, we linearly perturbed the single neutron star equilibrium system to model its radial oscillations. We then solved the entire coupled system of partial differential equations to obtain the frequencies of the oscillations. The sound speed in the equations as the gradient of pressure with respect to density, introduced stiffness into the system as $C_s \to 0$ towards the surface of the star.

The different mass-radius diagrams for these EoS indicated that the maximum masses from the IMEX scheme were consistent with the existing literature [132, 133]. Proving that the R-squared model is a viable model to extend general relativity for certain values of α.

The frequencies obtained from the FFT of the solution were verified with the eigenfrequencies from the Sturm-Liouville problem. The IMEX scheme frequencies proved to be consistent with the eigenfrequencies.

In the numerical relativity field, there is vast development of codes that solve problems in cosmology and astrophysics. In this thesis, tested the implementation of IMEX schemes to deal with stiffness, and successfully gave out accurate results for both in GR and $f(R)$. The IMEX scheme used in this thesis, can be used to test codes in the numerical relativity field, especially as testbeds for hydrodynamic codes that are used to model binary star mergers or collapse of supernovae. This thesis forms part of a larger goal to develop a high order code capable of simulating non linear structure formation in cosmology and binary neutron star mergers in theories beyond GR.

Acknowledgements

I would like to thank my super kind supervisor, Dr Bishop Mongwane, for all of his patience that he had with me while completing this thesis, for his consistency in always being there nudging me in the right direction and sitting down with me to work through code bugs. Lastly, I would like to thank him and Dr Kurt van der Heyden, for the financial help they provided for me throughout the degree. Thank you to my family for the daily calls and the never ending support and confidence they have given me. A final thank you to Sue Nyamnjoh for offering her sharp skill to proofread my drafts.

Chapter 8

Bibliography

[1] Riess, A. G., *et. al* (1998). Observational evidence from supernovae for an accelerating universe and a cosmological constant. The Astronomical Journal, 116(3), 1009.

[2] Perlmutter, S., *et. al* (1999). Measurements of Ω and Λ from 42 high-redshift supernovae. The Astrophysical Journal, 517(2), 565.

[3] Tegmark, M., *et. el* (2006). Cosmological constraints from the SDSS luminous red galaxies. Physical Review D, 74(12), 123507.

[4] Spergel, D. N., *et. al* (2003). First-year Wilkinson Microwave Anisotropy Probe (WMAP)* observations: determination of cosmological parameters. The Astrophysical Journal Supplement Series, 148(1), 175.

[5] Hut, P. (1977). Limits on masses and number of neutral weakly interacting particles. Physics Letters B, 69(1), 85-88.

[6] Holman, R., Lazarides, G., & Shafi, Q. (1983). Axions and the dark matter of the universe. Physical Review D, 27(4), 995.

[7] Uzan, J. P. (2007). The acceleration of the universe and the physics behind it. General Relativity and Gravitation, 39(3), 307-342.

[8] Copeland, E. J., Sami, M., & Tsujikawa, S. (2006). Dynamics of dark energy. International Journal of Modern Physics D, 15(11), 1753-1935.

[9] Weyl, H. (1919). A new extension of the theory of relativity. Annals of Physics , 364 (10), 101-133.

[10] Barrow, J. D., & Cotsakis, S. (1988). Inflation and the conformal structure of higher-order gravity theories. Physics Letters B, 214(4), 515-518.

[11] Barrow, J. D., & Ottewill, A. C. (1983). The stability of general relativistic cosmological theory. Journal of Physics A: Mathematical and General, 16(12), 2757.

[12] Hu, W., & Sawicki, I. (2007). Models of f (R) cosmic acceleration that evade solar system tests. Physical Review D, 76(6), 064004.

[13] Lattimer, J. M., & Prakash, M. (2001). Neutron star structure and the equation of state. The Astrophysical Journal, 550(1), 426.

[14] Abbott, B. P., *et. al* (2016). Observation of gravitational waves from a binary black hole merger. Physical review letters, 116(6), 061102.

[15] ABBOTT, B., *et. al* (2017). GW170104: Observation of a 50-Solar-Mass Binary Black Hole Coalescence at Redshift 0.2. Phys. Rev. Let, 118.

[16] Abbott, B. P., *et. al* (2016). GW151226: observation of gravitational waves from a 22-solar-mass binary black hole coalescence. Physical review letters, 116(24), 241103.

[17] Abbott, R., *et. al* (2020). GW190814: gravitational waves from the coalescence of a 23 solar mass black hole with a 2.6 solar mass compact object. The Astrophysical Journal Letters, 896(2), L44.

[18] Shibata, M., Zhou, E., Kiuchi, K., & Fujibayashi, S. (2019). Constraint on the maximum mass of neutron stars using GW170817 event. Physical Review D, 100(2), 023015.

[19] Mastrogiovanni, S., Steer, D. A., & Barsuglia, M. (2020). Joint tests of cosmology and modified gravity in light of GW170817. arXiv e-print arXiv:2004.06102.

[20] Mastrogiovanni, S., Haegel, L., Karathanasis, C., Magana-Hernandez, I., & Steer, D. A. (2020). Gravitational wave friction in light of GW170817 and GW190521. arXiv e-print arXiv:2010.04047.

[21] Ezquiaga, J. M., & Zumalacárregui, M. (2017). Dark energy after GW170817: dead ends and the road ahead. Physical review letters, 119(25), 251304.

[22] Gogoi, D. J., & Goswami, U. D. (2020). A new f (R) Gravity Model and properties of Gravitational Waves in it. arXiv e-print arXiv:2006.04011.

[23] Okounkova, M., Stein, L. C., Scheel, M. A., & Teukolsky, S. A. (2019). Numerical binary black hole collisions in dynamical Chern-Simons gravity. Physical Review D, 100(10), 104026.

[24] Witek, H., Gualtieri, L., & Pani, P. (2020). Towards numerical relativity in scalar Gauss-Bonnet gravity: 3+ 1 decomposition beyond the small-coupling limit. arXiv e-print arXiv:2004.00009.

[25] Cao, Z., Galaviz, P., & Li, L. F. (2013). Binary black hole mergers in f (R) theory. Physical Review D, 87(10), 104029.

[26] Tolman, R. C. (1939). Static solutions of Einstein's field equations for spheres of fluid. Physical Review, 55(4), 364.

[27] Tolman, R. C. (1934). Effect of inhomogeneity on cosmological models. Proceedings of the national academy of sciences of the United States of America, 20(3), 169.

[28] Caroll, S. M. c2004: Spacetime and geometry: An introduction to general relativity. P.–, SanFrancisco: Addition Wesley.

[29] Freedman, W. L., Madore, B. F., Gibson, B. K., Ferrarese, L., Kelson, D. D., Sakai, S.,& Huchra, J. P. *et. al* (2001). Final results from the Hubble Space Telescope key project to measure the Hubble constant. The Astrophysical Journal, 553(1), 47.

[30] Thorne, K. S., Misner, C. W., & Wheeler, J. A. (2000). Gravitation. Freeman.

[31] Oppenheimer, J. R., & Volkoff, G. M. (1939). On massive neutron cores. Physical Review, 55(4), 374.

[32] Miller, M. C. (2004). Introduction to neutron stars. University of Maryland, College Park.

[33] Buchdahl, H. A. (1970). Non-linear Lagrangians and cosmological theory. Monthly Notices of the Royal Astronomical Society, 150(1), 1-8.

[34] Koivisto, T. (2006). A note on covariant conservation of energy–momentum in modified gravities. Classical and Quantum Gravity, 23(12), 4289.

[35] Brans, C., & Dicke, R. H. (1961). Mach's principle and a relativistic theory of gravitation. Physical review, 124(3), 925.

[36] O'Hanlon, J. (1972). Intermediate-range gravity: a generally covariant model. Physical Review Letters, 29(2), 137.

[37] Teyssandier, P., & Tourrenc, P. (1983). The Cauchy problem for the R+ R 2 theories of gravity without torsion. Journal of mathematical physics, 24(12), 2793-2799.

[38] Wands, D. (1994). Extended gravity theories and the Einstein–Hilbert action. Classical and Quantum Gravity, 11(1), 269.

[39] Mongwane, B. (2017). Characteristic formulation for metric f (R) gravity. Physical Review D, 96(2), 024028.

[40] Stephani, H. (2004). Relativity: An introduction to special and general relativity. Cambridge university press.

[41] York Jr, J. W. (1979). Kinematics and dynamics of general relativity. Sources of gravitational radiation, 83-126.

[42] Arnowitt, R. L., Deser, S. D., & Misner, C. W. (1962). The dynamics of general relativity (No. gr-qc/0405109).

[43] Alcubierre, M. (2008). Introduction to 3+ 1 numerical relativity (Vol. 140). Oxford University Press.

[44] Rezzolla, L., & Zanotti, O. (2013). Relativistic hydrodynamics. Oxford University Press.

[45] Radice, D. (2013). Advanced numerical approaches in the dynamics of relativistic flows. (Doctoral dissertation, The Leibniz University Hannover).

[46] Ott, C. D. (2007). Stellar Iron Core Collapse in 3+ 1 General Relativity and The Gravitational Wave Signature of Core-Collapse Supernovae. (Doctoral dissertation, University of Potsdam).

[47] York Jr, J. W. (1973). Conformally invariant orthogonal decomposition of symmetric tensors on Riemannian manifolds and the initial-value problem of general relativity. Journal of Mathematical Physics, 14(4), 456-464.

[48] Alcubierre, M., Allen, G., Brugmann, B., Seidel, E., & Suen, W. M. (2000). Towards an understanding of the stability properties of the 3+ 1 evolution equations in general relativity. Physical Review D, 62(12), 124011.

[49] Gundlach, C., & Martin-Garcia, J. M. (2004). Symmetric hyperbolicity and consistent boundary conditions for second-order Einstein equations. Physical Review D, 70(4), 044032.

[50] Gundlach, C., & Martin-Garcia, J. M. (2006). Hyperbolicity of second order in space systems of evolution equations. Classical and Quantum Gravity, 23(16), S387.

[51] Shibata, M., & Nakamura, T. (1995). Evolution of three-dimensional gravitational waves: Harmonic slicing case. Physical Review D, 52(10), 5428.

[52] Baumgarte, T. W., & Shapiro, S. L. (1998). Numerical integration of Einstein's field equations. Physical Review D, 59(2), 024007.

[53] Alic, D., Bona-Casas, C., Bona, C., Rezzolla, L., & Palenzuela, C. (2012). Conformal and covariant formulation of the Z4 system with constraint-violation damping. Physical Review D, 85(6), 064040.

[54] Bona, C., Ledvinka, T., Palenzuela, C., & Zacek, M. (2003). General-covariant evolution formalism for numerical relativity. Physical Review D, 67(10), 104005.

[55] Lindblom, L., Scheel, M. A., Kidder, L. E., Owen, R., & Rinne, O. (2006). A new generalized harmonic evolution system. Classical and Quantum Gravity, 23(16), S447.

[56] Abrahams, A., Anderson, A., Choquet-Bruhat, Y., & York Jr, J. W. (1995). Einstein and Yang-Mills theories in hyperbolic form without gauge fixing. Physical review letters, 75(19), 3377.

[57] Friedrich, H. (1996). Hyperbolic reductions for Einstein's equations. Classical and Quantum Gravity, 13(6), 1451.

[58] Abrahams, A., Anderson, A., Choquet-Bruhat, Y., & York Jr, J. W. (1997). Geometrical hyperbolic systems for general relativity and gauge theories. Classical and Quantum Gravity, 14(1A), A9.

[59] Nakamura, T., Oohara, K., & Kojima, Y. (1987). General relativistic collapse to black holes and gravitational waves from black holes. Progress of Theoretical Physics Supplement, 90, 1-218.

[60] Sarbach, O., Calabrese, G., Pullin, J., & Tiglio, M. (2002). Hyperbolicity of the Baumgarte-Shapiro-Shibata-Nakamura system of Einstein evolution equations. Physical Review D, 66(6), 064002.

[61] Kidder, L. E., Scheel, M. A., & Teukolsky, S. A. (2001). Extending the lifetime of 3D black hole computations with a new hyperbolic system of evolution equations. Physical Review D, 64(6), 064017.

[62] Nagy, G., Ortiz, O. E., & Reula, O. A. (2004). Strongly hyperbolic second order Einstein's evolution equations. Physical Review D, 70(4), 044012.

[63] Baumgarte, T. W.,& Shapiro, S. L. (2003). Numerical relativity and compact binaries. Physics Reports, 376(2), 41-131.

[64] Hawking, S. W., & Ellis, G. F. R. (1973). The large scale structure of space-time (Vol. 1). Cambridge university press.

[65] York Jr, J. W. (1979). Kinematics and dynamics of general relativity. Sources of gravitational radiation, 83-126.

[66] Struwe, M. (1989). Plateau's Problem and the Calculus of Variations. (MN-35):. PRINCETON, NEW JERSEY: Princeton University Press. doi:10.2307/j.ctt7zv371

[67] Smarr, L., & York Jr, J. W. (1978). Kinematical conditions in the construction of spacetime. Physical Review D, 17(10), 2529.

[68] Bona, C., & Massó, J. (1988). Harmonic synchronizations of spacetime. Physical Review D, 38(8), 2419.

[69] Bona, C., & Massó, J. (1989). Einstein's evolution equations as a system of balance laws. Physical Review D, 40(4), 1022.

[70] Bona, C., & Massó, J. (1992). Hyperbolic evolution system for numerical relativity. Physical review letters, 68(8), 1097.

[71] Bona, C., & Massó, J. (1993). Numerical relativity: Evolving spacetime. International Journal of Modern Physics C, 4(04), 883-907.

[72] Bona, C., Masso, J., Seidel, E., & Stela, J. (1995). New formalism for numerical relativity. Physical Review Letters, 75(4), 600.

[73] Anninos, P., Massó, J., Seidel, E., Suen, W. M., & Towns, J. (1995). Three-dimensional numerical relativity: The evolution of black holes. Physical Review D, 52(4), 2059.

[74] Arbona, A., Bona, C., Massó, J., & Stela, J. (1999). Robust evolution system for numerical relativity. Physical Review D, 60(10), 104014.

[75] Broglie, L. D. (1924). XXXV. A tentative theory of light quanta. The London, Edinburgh, and Dublin Philosophical Magazine and Journal of Science, 47(278), 446-458.

[76] Landau, L. D., & Lifshitz, E. M. (1959). Fluid mechanics: Course of Theoretical Physics. Pergamon Press.

[77] Lichnerowicz, A. (1967). Relativistic hydrodynamics and magnetohydrodynamics: lectures on the existence of solutions. W.A. Benjamin, Inc.

[78] Von Neumann, J., & Richtmyer, R. D. (1950). A method for the numerical calculation of hydrodynamic shocks. Journal of applied physics, 21(3), 232-237.

[79] Font, J. A. (2008). Numerical hydrodynamics and magnetohydrodynamics in general relativity. Living reviews in relativity, 11(1), 7.

[80] Lax, P., & Wendroff, B. (1958). Systems of conservation laws (No. LA-2285). Los Alamos Scientific Lab., N. Mex..

[81] Font, J. A., Miller, M., Suen, W. M., & Tobias, M. (2000). Three-dimensional numerical general relativistic hydrodynamics: Formulations, methods, and code tests. Physical Review D, 61(4), 044011.

[82] Burden, R. L., & Faires, J. D. (1997). Numerical Analysis, Brooks. Cole, Belmont, CA.

[83] Mongwane, B. (2014). Problems in Cosmology and Numerical Relativity. (Doctoral dissertation, University of Cape Town).

[84] Press, W. H., Teukolsky, S. A., Vetterling, W. T., & Flannery, B. P. (1988). Numerical recipes in C.

[85] Courant, R., Friedrichs, K., & Lewy, H. (1928). Über die partiellen Differenzengleichungen der mathematischen Physik. Mathematische annalen, 100(1), 32-74.

[86] Courant, R., Friedrichs, K., & Lewy, H. (1967). On the partial difference equations of mathematical physics. IBM journal of Research and Development, 11(2), 215-234.

[87] Kreiss, H., & Oliger, J. (1973). Methods for the approximate solution of time dependent problems (No. 10). International Council of Scientific Unions, World Meteorological Organization.

[88] Runge, C. (1895). Über die numerische Auflösung von Differentialgleichungen. Mathematische Annalen, 46(2), 167-178.

[89] Kutta, W. (1901). Beitrag zur naherungsweisen Integration totaler Differentialgleichungen. Z. Math. Phys., 46, 435-453.

[90] Kreiss, H. O., & Scherer, G. (1992). Method of lines for hyperbolic differential equations. SIAM Journal on Numerical Analysis, 29(3), 640-646.

[91] Butcher, J. C. (1985). The non-existence of ten stage eighth order explicit Runge-Kutta methods. BIT Numerical Mathematics, 25(3), 521-540.

[92] Fehlberg, E. (1969). Low-order classical Runge-Kutta formulas with stepsize control and their application to some heat transfer problems (Vol. 315). NASA Technical Report 315.

[93] Cash, J. R., & Karp, A. H. (1990). A variable order Runge-Kutta method for initial value problems with rapidly varying right-hand sides. ACM Transactions on Mathematical Software (TOMS), 16(3), 201-222.

[94] Dormand, J. R., & Prince, P. J. (1980). A family of embedded Runge-Kutta formulae. Journal of computational and applied mathematics, 6(1), 19-26.

[95] Butcher, J. C., & Goodwin, N. (2008). Numerical methods for ordinary differential equations (Vol. 2). New York: wiley.

[96] Ŝolín, P. (2005). Partial differential equations and the finite element method (Vol. 73). John Wiley & Sons.

[97] Hairer, E., Nørsett, S. P., & Wanner, G. (1993). Solving ordinary differential equations I. Nonstiff problems (Vol. 8) Springer-Verlag Berlin Heidelberg.

[98] Harier, E., & Wanner, G. (1991). Solving ordinary differential equations II: stiff and differential algebraic problems. Springer Verlag.

[99] Dahlquist, G. G. (1963). A special stability problem for linear multistep methods. BIT Numerical Mathematics, 3(1), 27-43.

[100] Robertson, H. H. (1966). The solution of a set of reaction rate equations. Numerical analysis: an introduction, Academic Press: London, UK.

[101] Hall, G., & Higham, D. J. (1988). Analysis of stepsize selection schemes for Runge-Kutta codes. IMA journal of numerical analysis, 8(3), 305-310.

[102] Alexander, R. (1977). Diagonally implicit Runge–Kutta methods for stiff ODE's. SIAM Journal on Numerical Analysis, 14(6), 1006-1021.

[103] Pareschi, L., & Russo, G. (2005). Implicit–explicit Runge–Kutta schemes and applications to hyperbolic systems with relaxation. Journal of Scientific computing, 25(1), 129-155.

[104] Gottlieb, S., Shu, C. W., & Tadmor, E. (2001). Strong stability-preserving high-order time discretization methods. SIAM review, 43(1), 89-112.

[105] Harten, A. (1983). High resolution schemes for hyperbolic conservative laws. J Comp Phys, 49, 357-393.

[106] Godunov, S. K. (1959). A difference method for numerical calculation of discontinuous solutions of the equations of hydrodynamics. Matematicheskii Sbornik, 89(3), 271-306.

[107] B. van Leer, Towards the ultimate conservative difference scheme V. A second order sequel to Godunov's method, J. Comput. Phys., 32 (1979), pp. 101–136.

[108] Colella, P., & Woodward, P. R. (1984). The piecewise parabolic method (PPM) for gas-dynamical simulations. Journal of computational physics, 54(1), 174-201.

[109] Shu, C. W. (2009). High order weighted essentially nonoscillatory schemes for convection dominated problems. SIAM review, 51(1), 82-126.

[110] Harten, A., Engquist, B., Osher, S., & Chakravarthy, S. R. (1987). Uniformly high order accurate essentially non-oscillatory schemes, III. In Upwind and high-resolution schemes (pp. 218-290). Springer, Berlin, Heidelberg.

[111] Chi-Wang Shu (2011) WENO methods. Scholarpedia, 6(5):9709.

[112] Liu, X. D., Osher, S., & Chan, T. (1994). Weighted essentially non-oscillatory schemes. Journal of computational physics, 115(1), 200-212.

[113] Shu, C. W. (1990). Numerical experiments on the accuracy of ENO and modified ENO schemes. Journal of Scientific Computing, 5(2), 127-149.

[114] Shu, C. W. (1998). Essentially non-oscillatory and weighted essentially non-oscillatory schemes for hyperbolic conservation laws. In Advanced numerical approximation of nonlinear hyperbolic equations (pp. 325-432). Springer, Berlin, Heidelberg.

[115] Jiang, G. S., & Shu, C. W. (1996). Efficient implementation of weighted ENO schemes. Journal of computational physics, 126(1), 202-228.

[116] Lu, D., Chen, S., & Zhang, Y. T. (2018). Third order WENO scheme on sparse grids for hyperbolic equations. arXiv e-print arXiv:1804.00725.

[117] Dolgov, A. D., & Kawasaki, M. (2003). Can modified gravity explain accelerated cosmic expansion?. Physics Letters B, 573, 1-4.

[118] Núnez, A., & Solganik, S. (2004). The content of f (R) gravity. arXiv e-print hep-th/0403159.

[119] Nojiri, S. I., & Odintsov, S. D. (2006). Modified f (R) gravity consistent with realistic cosmology: From a matter dominated epoch to a dark energy universe. Physical Review D, 74(8), 086005.

[120] Capozziello, S., Nojiri, S. I., Odintsov, S. D., & Troisi, A. (2006). Cosmological viability of f (R)-gravity as an ideal fluid and its compatibility with a matter dominated phase. Physics Letters B, 639(3-4), 135-143.

[121] Odintsov, S. D., Oikonomou, V. K., & Sebastiani, L. (2017). Unification of constant-roll inflation and dark energy with logarithmic R2-corrected and exponential F (R) gravity. Nuclear Physics B, 923, 608-632.

[122] Starobinsky, A. A. (1980). A new type of isotropic cosmological models without singularity. Physics Letters B, 91(1), 99-102.

[123] De Felice, A., & Tsujikawa, S. (2010). f (R) theories. Living Reviews in Relativity, 13(1), 3.

[124] de La Cruz-Dombriz, A., Dobado, A., & Maroto, A. L. (2008). Evolution of density perturbations in f (R) theories of gravity. Physical Review D, 77(12), 123515.

[125] Cooney, A., DeDeo, S., & Psaltis, D. (2010). Neutron stars in f (R) gravity with perturbative constraints. Physical Review D, 82(6), 064033.

[126] Kase, R., & Tsujikawa, S. (2019). Neutron stars in f (R) gravity and scalar-tensor theories. Journal of Cosmology and Astroparticle Physics, 2019(09), 054.

[127] Astashenok, A. V., Capozziello, S., & Odintsov, S. D. (2013). Further stable neutron star models from f (R) gravity. Journal of Cosmology and Astroparticle Physics, 2013(12), 040.

[128] Demorest, P. B., Pennucci, T., Ransom, S. M., Roberts, M. S. E., & Hessels, J. W. T. (2010). A two-solar-mass neutron star measured using Shapiro delay. nature, 467(7319), 1081-1083.

[129] Antoniadis, J., Freire, P. C., Wex, N., Tauris, T. M., Lynch, R. S., van Kerkwijk, M. H., & Hessels, J. W. *et. al* (2013). A massive pulsar in a compact relativistic binary. Science, 340(6131).

[130] Abbott, B. P., *et. al* (2017). GW170817: observation of gravitational waves from a binary neutron star inspiral. Physical Review Letters, 119(16), 161101.

[131] Rezzolla, L., Most, E. R., & Weih, L. R. (2018). Using gravitational-wave observations and quasi-universal relations to constrain the maximum mass of neutron stars. The Astrophysical Journal Letters, 852(2), L25.

[132] Yazadjiev, S. S., Doneva, D. D., Kokkotas, K. D., & Staykov, K. V. (2014). Non-perturbative and self-consistent models of neutron stars in R-squared gravity. Journal of Cosmology and Astroparticle Physics, 2014(06), 003.

[133] Astashenok, A. V., Odintsov, S. D., & de la Cruz-Dombriz, Á. (2017). The realistic models of relativistic stars in f (R)= R+ αR 2 gravity. Classical and Quantum Gravity, 34(20), 205008.

[134] Resco, M. A., de la Cruz-Dombriz, Á., Estrada, F. J. L., & Castrillo, V. Z. (2016). On neutron stars in f (R) theories: Small radii, large masses and large energy emitted in a merger. Physics of the dark universe, 13, 147-161.

[135] Goswami, R., Maharaj, S. D., & Nzioki, A. M. (2015). Buchdahl-Bondi limit in modified gravity: Packing extra effective mass in relativistic compact stars. Physical Review D, 92(6), 064002.

[136] Ganguly, A., Gannouji, R., Goswami, R., & Ray, S. (2014). Neutron stars in the Starobinsky model. Physical Review D, 89(6), 064019.

[137] Nzioki, A. M., Goswami, R., & Dunsby, P. K. (2014). Jebsen-Birkhoff theorem and its stability in f (R) gravity. Physical Review D, 89(6), 064050.

[138] Ganguly, A., Gannouji, R., Goswami, R., & Ray, S. (2014). Neutron stars in the Starobinsky model. Physical Review D, 89(6), 064019.

[139] LORENE: Equations of state. (2005). LORENE. `https://lorene.obspm.fr/Refguide/group__EoS.html`

[140] Douchin, F., & Haensel, P. (2001). A unified equation of state of dense matter and neutron star structure. Astronomy & Astrophysics, 380(1), 151-167.

[141] Friedman, B., & Pandharipande, V. R. (1981). Hot and cold, nuclear and neutron matter. Nuclear Physics A, 361(2), 502-520.

[142] AKMAL, A., Pandharipande, V. R.,& Ravenhall, D. G. (1998). Equation of state of nucleon matter and neutron star structure. Physical Review C, 58(3), 1804.

[143] Balberg, S., Farrar, G. R., & Piran, T. (2001). Neutron stars with a stable, light supersymmetric baryon. The Astrophysical Journal Letters, 548(2), L179.

[144] Baldo, M., Bombaci, I. G. N. A. Z. I. O., & Burgio, G. F. (1997). Microscopic nuclear equation of state with three-body forces and neutron star structure. arXiv e-print astro-ph/9707277.

[145] Bombaci, I., Prakash, M., Prakash, M., Ellis, P. J., Lattimer, J. M., & Brown, G. E. (1995). Newborn hot neutron stars. Nuclear Physics A, 583, 623-628.

[146] Chandrasekhar, S. (1964). Dynamical instability of gaseous masses approaching the Schwarzschild limit in general relativity. Physical Review Letters, 12(4), 114.

[147] B. K. Harrison, K. S. Thorne, M. Wakano, J. A. Wheeler, Gravitation Theory and Gravitational Collapse (Univ. of Chicago Press, Chicago, 1965).

[148] Ruoff, J. (2000). The numerical evolution of neutron star oscillations. (Doctoral dissertation, University of Potsdam). Arxiv e-print gr-qc/0010041.

[149] Passamonti, A. (2006). Non-linear oscillations of compact stars and gravitational waves. (Doctoral dissertation, University of Portsmouth).

[150] Bardeen, J. M., Thorne, K. S., & Meltzer, D. W. (1966). A catalogue of methods for studying the normal modes of radial pulsation of general-relativistic stellar models. The Astrophysical Journal, 145, 505.

[151] Chanmugam, G. (1977). Radial oscillations of zero-temperature white dwarfs and neutron stars below nuclear densities. The Astrophysical Journal, 217, 799-808.

[152] Glass, E. N., & Lindblom, L. (1983). The radial oscillations of neutron stars. The Astrophysical Journal Supplement Series, 53, 93-103.

[153] Väth, H. M., & Chanmugam, G. (1992). Radial oscillations of neutron stars and strange stars. Astronomy and Astrophysics, 260, 250-254.

[154] Kokkotas, K., & Ruoff, J. (2001). Radial oscillations of relativistic stars. Astronomy & Astrophysics, 366(2), 565-572.

[155] Tsang, D., Read, J. S., Hinderer, T., Piro, A. L., & Bondarescu, R. (2012). Resonant shattering of neutron star crusts. Physical Review Letters, 108(1), 011102.

[156] Chirenti, C., Gold, R., & Miller, M. C. (2017). Gravitational waves from f-modes excited by the inspiral of highly eccentric neutron star binaries. The Astrophysical Journal, 837(1), 67.

[157] Yoshida, S., & Kojima, Y. (1997). Accuracy of the relativistic Cowling approximation in slowly rotating stars. Monthly Notices of the Royal Astronomical Society, 289(1), 117-122.

[158] Font, J. A., *et. al* (2002). Three-dimensional numerical general relativistic hydrodynamics. II. Long-term dynamics of single relativistic stars. Physical Review D, 65(8), 084024.

Appendix A

Root-Finding Methods

In solving our field equations which we'll derive in the next section, we combined our ODE solver with a root finding method for the Ricci scalar function. Here we briefly present an overview of some of these methods, an interested reader can consult most introductory numerical relativity textbooks like [84, 102] which cover these methods in depths. We suppose for an arbitrary real function $f(x)$, we are looking for critical points x_{crit} that solve the problem

$$f(x) = 0, \tag{A.1}$$

as some functions are difficult to solve analytically. The first root finding method we consider the *bisection* method, which is a two-point method such that two starting guesses x_i and x_j. A logical step in this method is that it requires the values $f(x_i)$ and $f(x_j)$, to have opposite signs such that

$$f(x_i)f(x_j) \leq 0.$$

The update step is calculated from the midpoint of the previous two guesses as

$$x_k = \frac{x_i + x_j}{2}.$$

In the case that x_k is not the root then based on the sign of $f(x_k)$, the next guess is calculated by assigning x_k to x_i or x_j if $sign(f(x_k)) = sign(f(x_i))$ or $sign(f(x_k)) = sign(f(x_j))$ respectively. It is advisable that there an additional tolerance requirement on $|f(x_k)|$ proximity to the origin. As the update step may jump over the root after only coming close to it even though this method always converges to the root but may do so slowly.

A similar method that uses the same logical step is the *regular falsi* method, although its update step is more intricate. When calculating the next guess, it also considers the values of the function at the initial two guesses x_i and x_j such that if $f(x_i)f(x_j) \leq 0$, then next root guess is obtained as

$$x_k = x_i - f(x_i)\frac{(x_j - x_i)}{f(x_j) - f(x_i)}.$$

Similarly to the bisection method, the sign of $f(x_k)$ determines the role of x_k in the next iteration, suppose x_k is not the root. This method can be set iterate until a certain tolerance is reached. Its convergence is far better than that of the bisection method, but its speed is dependant on the gradient of the considered function.

The *secant* method uses the update step to the regular falsi method, although it does not take the sign of the functions into consideration when updating. Given two starting points x_i and x_{i-1}, the secant method calculates the next guess using the formula

$$x_{i+1} = x_{i-1} - f(x_{i-1})\frac{(x_i - x_{i-1})}{f(x_i) - f(x_{i-1})},$$

and the iteration is repeated for a finite number of times, unless the there is a tolerance on $|f(x_k)|$ set.

The last but not least root finding method, is sort of a combination of all the above mentioned methods and it is called ***Ridder's*** method. Given two starting points x_i and x_j whose function values have opposite signs in [x_i,x_j], the Ridder's method considers the midpoint between these points

$$x_k = \frac{x_i + x_j}{2},$$

such that with the knowledge of $f(x_k)$ we can calculate the next guess using the formula

$$x_\ell = x_k + (x_k - x_i)\frac{(f(x_i) - f(x_j))f(x_k)}{\sqrt{f(x_k)^2 - f(x_i)f(x_j)}}. \tag{A.2}$$

The sign of $f(x_{\ell)}$ determines the region where root is located, and the method is repeated for the region [x_i,x_ℓ] if $f(x_{\ell)} > 0$ or [x_ℓ,x_j] if $f(x_{\ell)} < 0$. The Ridders method has much better convergence compared to the other methods we have mentioned.

Appendix B

Hyperbolic Partial Differential Equations

We have encountered more hyperbolic first equations so far like the ADM or hydrodynamic equations, hence in this section we will consider the first order hyperbolic equations which are the scalar form of (3.71) given by the 1-d advection equation

$$\partial_t u + v u_x = 0, \tag{B.1}$$

where v is the constant velocity of our "fluid-wave" and [84] we already know that the general solution that satisfies this equation has the form

$$u(t, x) = u(x - vt). \tag{B.2}$$

We continue to discretize our spacetime into a grid of points of uniform grid spacing both for time and space using (4.1) and (4.2) to denote these points and levels. Then we use the centered differencing method to represent the spatial derivative such that

$$(u_x)_i^n = \frac{u_{i+1}^n - u_{i-1}^n}{2\Delta x} + \mathcal{O}(\Delta x^2) \tag{B.3}$$

where $u_i^n = u(t^n, x_i)$. For the representation of the time derivative, we use a one-sided *forward-time* differencing similar to (4.4) which gives us the first-order form

$$(\partial_t u)_i^n = \frac{u^{n+1} - u_j^n}{\Delta t} + \mathcal{O}(\Delta t). \tag{B.4}$$

Then substituting into the differential equation (B.1) and using the advantage of the forward-time scheme we solve for the next time level to find

$$u_i^{n+1} = u_i^n - \frac{v}{2}\frac{\Delta t}{\Delta x}(u_{i+1}^n - u_{i-1}^n). \tag{B.5}$$

This scheme is called the *forward-time centered-space* (FTCS) which is first-order in time and second-order in space and it is an example of an *explicit* scheme due to its advantage of using known quantities of the current time level n to obtain information about the next time level.

We need to know the stability properties of this presented scheme and to do so we employ the method called the *von Neumann stability analysis*. It is an efficient method at assessing the stability of the finite-difference schemes of the form

$$\boldsymbol{u}^{n+1} = \boldsymbol{A}\boldsymbol{u}^n, \tag{B.6}$$

where $\boldsymbol{A}$ is just an update as depicted and we assume the existence of a complete set of its eigenvectors such that the solution $\boldsymbol{u}^n$ can be written as a linear combination of them. Where the equations are Fourier transformed and the transformed version of the update matrix is called the *amplification matrix* $\hat{\boldsymbol{A}}$, such that the von Neumann stability condition requires the spectral radius of $\hat{\boldsymbol{A}}$ be less than or equal to 1. That is requiring that if we write the Fourier version of the solution as the summation of its eigenmodes such that

$$\boldsymbol{u}^n = \sum_k \xi^n e^{ikx}, \tag{B.7}$$

the amplification factor $\xi(k)$ has to satisfy

$$|\xi|^2 = \xi^* \xi \leq 1, \tag{B.8}$$

as it is a complex number dependant the real spatial wave number k. Although the von Neumann stability analysis is a local [44] method in the sense that we can assume that any variation around the elements of the update matrix is so slow throughout the evolution such that it is negligible, and additionally it assumes periodic boundary conditions to neglect any boundary effects.

Going back to the von Neumann stability analysis we use the eigenmode expansion (B.7) and absorb the initial spatial exponent into the amplification factor such that we substitute

$$u_m^n = \xi^n e^{ik(m\Delta x)}, \tag{B.9}$$

into (B.5), then we use the identity $(e^{iy} - e^{-iy}) = i2\sin y$ to simplify the equation further to get the amplification factor as

$$\xi(k) = 1 - i\frac{v}{2}\frac{\Delta t}{\Delta x} sin(k\Delta x), \tag{B.10}$$

with the square modulus of the above equation has

$$|\xi|^2 = 1 + v^2\left(\frac{\Delta t}{\Delta x}\right)^2 sin^2(k\Delta x). \tag{B.11}$$

The modulus violates the *von Neumann* criterion (B.8) for all values of k and we note that this is true for any value of Δx and Δt meaning that the FTCS scheme is unconditionally unstable and we cannot use it for the wave equation evolution, additionally the initial assumption about the velocity to be constant does not help. Although according to Lax and Friedrichs one can instead use the 2-norm of the finite-difference solution, which is basically the average of solution in the grid such that

$$u_i^n = \frac{u_{i+1}^n + u_{i-1}^n}{2} + \mathcal{O}(\Delta x^2), \tag{B.12}$$

and this substitution gives us the *Lax-Friedrichs* scheme as

$$u_i^{n+1} = \frac{1}{2}(u_{i+1}^n + u_{i-1}^n) - \frac{v}{2}\frac{\Delta t}{\Delta x}(u_{i+1}^n - u_{i-1}^n). \tag{B.13}$$

For which we perform the von Neumann stability analysis by substituting (B.9) and solve for the square modulus of the amplification factor similar to the FCTS to obtain

$$|\xi|^2 = cos^2(k\Delta x) + \left(\frac{v}{2}\frac{\Delta t}{\Delta x}\right)^2 sin^2(k\Delta x), \tag{B.14}$$

which satisfies the von Neumann criterion given that

$$\Delta t \leq \frac{\Delta x}{|v|}, \tag{B.15}$$

and this inequality that relates the time step Δt to the spatial separation Δx is known as the *Courant-Friedrichs-Lewy* (CFL) *condition* which was suggested a little before its time [85] and also revisited after the first generation of digital computers in [86]. The CFL condition ensures that when employing explicit, one-leveled schemes like the FTCS (B.5) or *Lax-Friedrichs* (B.13) schemes, the set of points that u_i^n depends on (*domain of dependence*) must never be larger than the set of points that determine u_i^n (*numerical domain of dependence*). Note that the inequality holds for the propagation speed of our wave such that it never surpass the numerical speed $\Delta x/\Delta t$ to maintain stability. Then given that the time step Δt is chosen to be sufficiently smaller than the spatial grid time, this makes the Lax-Friedrichs scheme conditionally stable.

We have to turn the instability of the FTCS scheme to a conditionally stable scheme by using the local average solution (B.12), although something something fundamental occurred and we note it by comparing the FTCS and Lax-Friedrichs schemes such that we rewrite them in the forms

$$\frac{u_i^{n+1} - u_i^n}{\Delta t} = -v\left(\frac{u_{i+1}^n - u_{i-1}^n}{2\Delta x}\right), \tag{B.16}$$

and

$$\frac{u^{n+1} - u_i^n}{\Delta t} = -v\left(\frac{u_{i+1}^n - u_{i-1}^n}{2\Delta x}\right) + \frac{(\Delta x)^2}{2\Delta t}\left(\frac{u_{i+1}^n - 2u_i^n + u_{i-1}^n}{(\Delta x)^2}\right), \tag{B.17}$$

respectively, and we notice that the second term on the right of the Lax-Friedrichs form (B.17) is a centered-difference of a second derivative, which makes (B.17) the finite-difference representation for the partial differential equation

$$\partial_t u + v\partial_x = Du_x^2, \tag{B.18}$$

where D is the spatial covariant derivative in 1-d, and the term on the right is called a diffusion term. Which is the term that was effectively added to the differential equation and resulted in a stable numerical scheme equivalent to the Lax-Friedrichs scheme. Obtaining this centered-difference term, we divided by Δx^2 such that the term is $\mathcal{O}(\Delta x)$, and therefore we guaranteed that in the continuum limit of $\Delta x \to 0$, the term goes to zero and we recover the true solution of the differential equation which is what makes the term purely numerical as compared to the artificial dissipation we have encountered in the previous chapter.

Considering the length scale L_s of our grid, we are interested in a large domain of dependence such that any scheme we choose is accurate for the scales that we are interested in $k\Delta x \ll 1$. In these said scales, the FTCS and Lax-Friedrichs schemes seem to have $\xi(k) \backsim 1$ which them both equally accurate, and respectively unstable and stable. Although for short scales such as $k\Delta x \backsim \frac{\pi}{2}$, we note that from the description of the eigenmodes (B.9) the unstable scheme (FTCS) will blow up and overshadow the true solutions, and the Lax-Scheme scheme will only be inaccurate due to disappearing wavelengths. This is called anomalous dispersion which is not really a problem it gets resolved with many grid points.

The presence of the diffusion term can be used when high frequency errors are worrisome in a particular scheme, if it is of higher order ($\partial_x^m,\ m \geq 4$) then it can damp outs the high frequency errors [83] in the scheme to destabilize integration of the differential equation. Kreiss and Oliger's work [87] is one example of this where they introduced a dissipation operator such that the diffusion term is multiplied by a 'dissipation coefficient' of small magnitude with the intent of regulating the dissipation operator on hyperbolic systems.

We have presented two one-level, explicit schemes that are both first order accurate in time, there are other finite-differencing schemes, one that improves on the CFL condition of the Lax-Friedrichs scheme by instead using a second-order temporal discretization called the *leapfrog scheme*, or the *Crank-Nicholson* scheme that is second-order in both time and space and also an explicit two-level scheme. The interested reader can refer to some numerical texts as they present them with such depth [44, 52].

Appendix C

Finite-Difference ENO Schemes

The work of essentially non-oscillatory schemes was pioneered by Harten *et al* in [110] which are based on reconstructing the numerical solution from interpolation polynomials and adaptive stencils. In section (4.1) we presented finite difference methods for hyperbolic PDEs. These schemes do not perform well when encountering discontinuities in the grid, resulting in oscillations around the discontinuity. ENO methods are uniformly higher order methods that handle discontinuities without any oscillations around the discontinuity. To illustrate the method, we consider the model problem (4.13) and, for simplicity, we omit the source terms

$$\frac{d}{dt}u = \partial_x F(u). \tag{C.1}$$

To obtain its spatially discretized finite-difference form while leaving the time dimension continuous, we assume a uniform grid with spacing Δx and that we can obtain a function $h(x)$ such that

$$F(u) = \frac{1}{\Delta x}\int_{x-\frac{\Delta x}{2}}^{x+\frac{\Delta x}{2}} h(\xi)d\xi, \tag{C.2}$$

which would imply that

$$\partial_x F(u) = \frac{1}{\Delta x}\left[h\left(x+\frac{\Delta x}{2}\right) - h\left(x-\frac{\Delta x}{2}\right)\right]. \tag{C.3}$$

Hence then at our grid points x_i we set

$$\hat{F}_{j\pm\frac{1}{2}} = h(x_{j\pm\frac{1}{2}}) + \mathcal{O}(\Delta x^k), \tag{C.4}$$

which then approximates the spatial derivative of the physical fluxes up the $k-th$ order accuracy such that the fully spatially discretized system is written as

$$\frac{d}{dt}u_j = \frac{1}{\Delta x}(\hat{F}_{j+\frac{1}{2}} - \hat{F}_{j-\frac{1}{2}}), \tag{C.5}$$

where the numerical flux functions $\hat{F}_{j\pm\frac{1}{2}}$ are a higher order approximation to the primitives (*i.e* anti-derivatives) functions $h(x)$. The numerical fluxes still have an implicit continuous dependence on time since the left-hand side is a full derivative of time.

We define an interval for the cells such that $I_i = [x_{i-\frac{1}{2}}, x_{i+\frac{1}{2}}]$, and we can use a union of these intervals to define a stencil S_j for the j−th cell as a portion of the grid such that

$$S_j = \bigcup_{i=j-\ell}^{j+r} I_i, \tag{C.6}$$

with r and ℓ cells to the right and left. The numerical flux functions in eq. (C.4) are approximated as point functions whose cell average gives us the approximate physical fluxes, although we require a point-wise representation of the numerical fluxes functions. We follow the reconstruction technique in [110] to obtain this representation. We first suppose a primitive function of $h(x)$ such that

$$H(x) = \int_{-\infty}^{x} h(\xi)d\xi, \tag{C.7}$$

which in terms of the physical fluxes definition (C.2) at point $x_{i+\frac{1}{2}}$, this primitive function can be rewritten as a summation of integrals over the cells I_i such that

$$H(x_{i+\frac{1}{2}}) = \sum_{j=-\infty}^{i} \int_{x_{j-\frac{1}{2}}}^{x_{j-\frac{1}{2}}} h(\xi)d\xi. \tag{C.8}$$

Clearly the primitive function $H(x)$ is a summation of the pointwise values of the physical flux functions $F(x_j) = F_i$ due to (C.2) such that

$$H(x_{i+\frac{1}{2}}) = \Delta x \sum_{j=-\infty}^{i} F_i. \tag{C.9}$$

Now the only quantity we require are the point values of the primitive function at the boundaries of the cells $h(x_{i+\frac{1}{2}})$ which we can obtain by finding a unique polynomial $P_i(x)$ of degree at most k that interpolates the primitive function $H(x_{i+\frac{1}{2}})$ in the stencil S_j with k points, such that the derivative of this polynomial $p_i(x)$ is a $(k-1)$-th order polynomial that interpolates the numerical fluxes by satisfying at the cell boundaries

$$p(x_{i+\frac{1}{2}}) = \hat{F}(x_{i+\frac{1}{2}}) + \mathcal{O}(\Delta x^k). \tag{C.10}$$

The ENO reconstruction method has resulted in a sequence of $(k-1)$-th order polynomials that interpolate the physical fluxes in the stencils S_j. So far we have based it on a fixed stencil such that shift to the left by ℓ applies to of the cells in the stencil. For piecewise smooth functions that do have discontinuities, using the fixed stencil leads to oscillatory effects of the physical fluxes around the discontinuities. As the stencil will contain points where (C.10) is not well defined. The ENO method employs an *adaptive stencil* that avoids the points of discontinuity in the stencil. Harten *et al* [110] suggested the interpolation function takes the form of the Lagrange interpolation function $P_i(x)$ at $k+1$ points such that

$$P_i(x) = \sum_{i=0}^{k} a_i H[x_{j-r-\frac{1}{2}}, ..., x_{j-r+i-\frac{1}{2}}], \tag{C.11}$$

where

$$a_i = \prod_{n=0}^{i-1} (x - x_{j-r+m-\frac{1}{2}}), \tag{C.12}$$

and the $j-$th divided difference of the primitive function $H(x)$ are given by

$$H[x_{j-r-\frac{1}{2}},...,x_{j-r+i-\frac{1}{2}}] = \frac{H[x_{j-r+\frac{1}{2}},...,x_{j-r+i-\frac{1}{2}}] - H[x_{j-r-\frac{1}{2}},...,x_{j-r+i-\frac{3}{2}}]}{x_{j-r+i-\frac{1}{2}} - x_{j-r-\frac{1}{2}}}. \tag{C.13}$$

Then the derivative of this function gives us the $(k-1)$-th interpolation function of the physical fluxes

$$p_i(x) = \sum_{i=1}^{k} a_i H[x_{j-r-\frac{1}{2}},...,x_{j-r+i-\frac{1}{2}}], \tag{C.14}$$

where now the constants are given by

$$a_i = \prod_{n=0,n\neq i}^{i-1} (x - x_{j-r+n-\frac{1}{2}}). \tag{C.15}$$

The next step is to cautiously build a stencil S_j such that the function $H(x)$ is smoothest in it compared to other possible stencils that may contain discontinuities. One does this by looking left and right of the $j-th$ cell starting with the stencil

$$\hat{S}_j = I_j, \tag{C.16}$$

assuming that $H(x)$ is smooth in this stencil, then its divided difference $H[x_{i-\frac{1}{2}}, x_{i+\frac{1}{2}}]$ form must be relatively smaller in this stencil. Then from here we can either add the left point $x_{j-\frac{3}{2}}$ or the right point $x_{j+\frac{3}{2}}$ in order to grow our stencil, which is simply having to choose between the two divided difference forms $H[x_{j-\frac{3}{2}}, x_{i+\frac{1}{2}}]$ and $H[x_{x_{i-\frac{1}{2}},x_{j+\frac{3}{2}}}]$ to include in the interpolation function (C.11). The pivotal point of the ENO method suggests that the criterion that must be met is that the next point to be included must have a smaller absolute divided difference such that if

$$|H[x_{j-\frac{3}{2}}, x_{i+\frac{1}{2}}]| < |H[x_{x_{i-\frac{1}{2}},x_{j+\frac{3}{2}}}]|, \tag{C.17}$$

then the next point to include is $x_{j-\frac{3}{2}}$, this results in the stencil

$$\hat{S}_j = \bigcup_{i=j-3/2}^{j+1/2} I_i. \tag{C.18}$$

This process is then done repeatedly for each and every point to be included, avoiding the discontinuous points in the grid up to the k points resulting in the stencil

$$S_j = \bigcup_{i=j-\ell}^{j+r} \hat{S}_i, \tag{C.19}$$

with the interpolation function (C.11) whose derivative $p_i(x)$ interpolates the physical fluxes in the same stencil up to $(k-1)$ order of accuracy. The function $p_i(x)$ contains the least oscillatory effects around the discontinuity due its coefficients being very small, and then this implies that the ENO method does not allow any local extrema in the function such that $p_i(x)$ is monotone in the cells with discontinuous points.